RESEARCH ARTICLE

Discovery, Preclinical Characterization, and Early Clinical Activity of JDQ443, a Structurally Novel, Potent, and Selective Covalent Oral Inhibitor of KRAS^{G12C}

Andreas Weiss[1], Edwige Lorthiois[1], Louise Barys[1], Kim S. Beyer[1], Claudio Bomio-Confaglia[1], Heather Burks[2], Xueying Chen[3], Xiaoming Cui[3], Ruben de Kanter[1], Lekshmi Dharmarajan[1], Carmine Fedele[2], Marc Gerspacher[1], Daniel Alexander Guthy[1], Victoria Head[1], Ashley Jaeger[2], Eloísa Jiménez Núñez[1], Jeffrey D. Kearns[2], Catherine Leblanc[1], Sauveur-Michel Maira[1], Jason Murphy[2], Helen Oakman[2], Nils Ostermann[1], Johannes Ottl[1], Pascal Rigollier[1], Danielle Roman[1], Christian Schnell[1], Richard Sedrani[1], Toshio Shimizu[4], Rowan Stringer[1], Andrea Vaupel[1], Hans Voshol[1], Peter Wessels[5], Toni Widmer[5], Rainer Wilcken[1], Kun Xu[3], Frederic Zecri[2], Anna F. Farago[2], Simona Cotesta[1], and Saskia M. Brachmann[1]

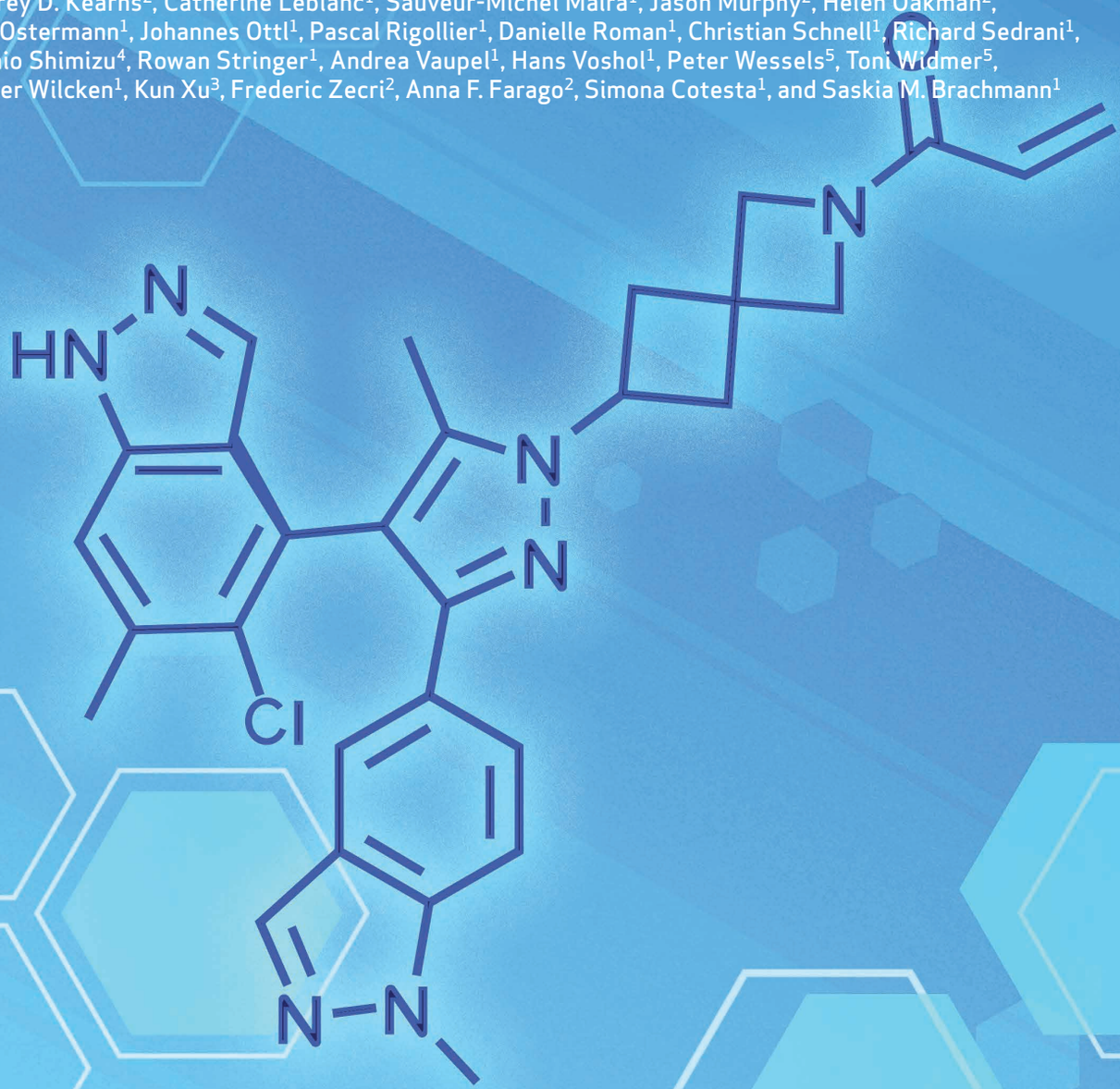

ABSTRACT Covalent inhibitors of KRAS^{G12C} have shown antitumor activity against advanced/metastatic *KRAS*^{G12C}-mutated cancers, though resistance emerges and additional strategies are needed to improve outcomes. JDQ443 is a structurally unique covalent inhibitor of GDP-bound KRAS^{G12C} that forms novel interactions with the switch II pocket. JDQ443 potently inhibits KRAS^{G12C}-driven cellular signaling and demonstrates selective antiproliferative activity in *KRAS*^{G12C}-mutated cell lines, including those with G12C/H95 double mutations. *In vivo*, JDQ443 induces AUC exposure-driven antitumor efficacy in *KRAS*^{G12C}-mutated cell-derived (CDX) and patient-derived (PDX) tumor xenografts. In PDX models, single-agent JDQ443 activity is enhanced by combination with inhibitors of SHP2, MEK, or CDK4/6. Notably, the benefit of JDQ443 plus the SHP2 inhibitor TNO155 is maintained at reduced doses of either agent in CDX models, consistent with mechanistic synergy. JDQ443 is in clinical development as monotherapy and in combination with TNO155, with both strategies showing antitumor activity in patients with *KRAS*^{G12C}-mutated tumors.

SIGNIFICANCE: JDQ443 is a structurally novel covalent KRAS^{G12C} inhibitor with a unique binding mode that demonstrates potent and selective antitumor activity in cell lines and *in vivo* models. In preclinical models and patients with *KRAS*^{G12C}-mutated malignancies, JDQ443 shows potent antitumor activity as monotherapy and in combination with the SHP2 inhibitor TNO155.

See related video: https://vimeo.com/720726054

INTRODUCTION

In healthy cells, RAS proteins regulate a number of intracellular signaling pathways associated with growth and differentiation, acting as molecular switches that cycle between an active state (ON) bound to guanosine triphosphate (GTP) and an inactive state (OFF) bound to guanosine diphosphate (GDP). Somatic *RAS* mutations were the first oncogenic mutations identified in human cancers (1) and are primarily comprised of gain-of-function missense alterations at codons 12, 13, or 61 that impair GTP hydrolysis to favor the protein's active state, resulting in increased activation of downstream signaling pathways linked to cell proliferation, cell survival, and tumorigenesis (2). KRAS is the most frequently mutated of the three RAS isoforms, with *KRAS* mutations commonly identified in pancreatic adenocarcinoma (PDAC; >90%; ref. 3), colorectal cancer (~40%; ref. 4), and non–small cell lung cancer (NSCLC; ~28%; ref. 5).

KRAS was long considered undruggable due to extremely strong avidity for intracellularly abundant guanine nucleotides, an apparent absence of targetable allosteric sites, and the clinical failure of attempts to target other critical aspects of KRAS functioning such as KRAS membrane attachment (6) or inhibition of downstream signaling in the absence of direct selective inhibition of the driver oncogene. However, one common KRAS oncogenic variant—a glycine-to-cysteine substitution at amino acid 12 (KRAS^{G12C}) that occurs in approximately 13% of lung adenocarcinomas, 4% of colon tumors, and smaller fractions of other cancers (7)—was recently found to be targetable by small-molecule inhibitors (8, 9).

The first *in vitro* demonstrations of targeted KRAS^{G12C} inactivation showed irreversible covalent modification of the GDP-bound KRAS^{G12C} cysteine-12 residue by two independent research groups utilizing different approaches. One group used a chloroacetamide GDP analogue with a membrane-permeable caged prodrug (8), and the other (9) used a series of vinyl sulfonamides and piperazyl acrylamides with allosteric binding to a pocket below the switch II region of the protein (SWIIP) that was initially identified earlier during the development of the noncovalent RAS GDP exchange inhibitor SCH-54292 (10–12), and subsequently observed through the interaction of the RAS homolog RalA with the bacterial protein C3bot (13). Allosteric binding and cysteine-12 modification resulted in trapping of KRAS^{G12C} in the inactive state, with prevention of Son of Sevenless (SOS)–mediated GTP nucleotide exchange and the subsequent impairment of RAF effector protein binding (9). These early acrylamide structures formed the basis of subsequent discovery efforts leading to the development of the compound ARS-853 (14), which validated the drug concept *in vitro* and demonstrated that KRAS^{G12C} is indeed still cycling in cells (15, 16), and

[1]Novartis Institutes for BioMedical Research, Basel, Switzerland. [2]Novartis Institutes for BioMedical Research, Cambridge, Massachusetts. [3]Novartis Pharmaceuticals Corporation, East Hanover, New Jersey. [4]National Cancer Center Hospital, Tokyo, Japan. [5]Novartis Pharma AG, Basel, Switzerland.

Note: Supplementary data for this article are available at Cancer Discovery Online (http://cancerdiscovery.aacrjournals.org/).

A. Weiss and E. Lorthiois contributed equally as co–lead authors of this article.

A.F. Farago, S. Cotesta, and S.M. Brachmann contributed equally as co–senior authors of this article.

Corresponding Authors: Saskia M. Brachman, Novartis Institutes for BioMedical Research (NIBR), WSJ-386/3/13.01, Kohlenstrasse 84, 4056 Basel, Switzerland. Phone: 41-616-9640-63; E-mail: saskia.brachmann@novartis.com; Anna F. Farago, NIBR, 250 Massachusetts Avenue, Cambridge, MA 02139. Phone: 617-871-8000; E-mail: anna.farago@novartis.com; and Simona Cotesta, NIBR, WSJ-386/13/10, Kohlenstrasse 84, 4056 Basel, Switzerland. Phone: 41-797-9792-70; E-mail: simona.cotesta@novartis.com

Cancer Discov 2022;12:1500–17

doi: 10.1158/2159-8290.CD-22-0158

the compound ARS-1620 (17), which showed the first *in vivo* validation in patient-derived mouse models of *KRAS*^{G12C}-mutated NSCLC and PDAC.

Several orally bioavailable small-molecule covalent KRAS^{G12C} inhibitors have subsequently entered clinical development, including sotorasib (AMG 510; ref. 18) and adagrasib (MRTX-849; ref. 19). Both also showed antitumor activity against *KRAS*^{G12C}-mutated tumors in early-phase clinical trials (20), leading to the accelerated approval of sotorasib by the FDA in May 2021 and conditional marketing authorization by the European Commission in January 2022. Nonetheless, there remains an ongoing need for improved clinical outcomes (21), especially since emerging data indicate multiple mechanisms of acquired resistance in patients treated with sotorasib or adagrasib (22–24), many of which involve RAS pathway reactivation. Consequentially, combination strategies are being explored, such as with inhibitors of upstream pathway components such as EGFR (25, 26) and SHP2 (ClinicalTrials.gov IDs NCT05054725 and NCT04330664) and downstream pathway components such as MEK (27), with the goal to further suppress RAS-mediated pathways and induce more potent and durable antitumor activity. However, clinical toxicity may limit specific combination strategies.

A chemically distinct KRAS^{G12C} inhibitor may offer unique advantages in combinations. Herein we report the discovery and characterization of JDQ443, a potent and selective, orally bioavailable covalent inhibitor of GDP-bound KRAS^{G12C} with a novel binding mode, designed to offer a structurally unique inhibitor with a distinct central core that occupies the SWIIP in a novel way to potentially enable unique clinical advantages. We present the *in vitro* and *in vivo* efficacy of JDQ443 both alone and in combination with inhibitors of RAS upstream and downstream signaling components. Furthermore, early clinical data show evidence of JDQ443 antitumor activity in *KRAS*^{G12C}-mutated tumors both as monotherapy and in combination with the SHP2 inhibitor TNO155.

RESULTS

Discovery of JDQ443, a Structurally Unique Covalent Inhibitor of KRAS^{G12C} with a Novel Binding Mode in SWIIP

JDQ443 was discovered by extensive optimization of a weak hit **[3]** (Fig. 1A) identified by *de novo* structure-based design, inspired by analyses of published and internal cocrystal structures of KRAS^{G12C} with **[1]** and **[2]** (Supplementary Fig. S1A and S1B). The importance of an indazole fragment was highlighted by **[1]** (Fig. 1A), which forms a hydrogen bond with the D69 side chain and the S65 backbone (water-mediated) and fills a hydrophobic region formed by V103, I100, M72, and Y96 (Supplementary Fig. S1A), whereas **[2]**, discovered from structure–activity relationship (SAR) exploration of a weak hit identified by a mass spectrometry (MS)–based screen (see Supplementary Methods; 3,315 molecules tested, 107 confirmed hits with single KRAS^{G12C} target modification and >50% modification after 2 hours at 50 μmol/L compound concentration), contained a phenyl acrylamide (Fig. 1A), which optimally orients the acrylamide moiety for reaction with cysteine-12 (Supplementary Fig. S1B). Subsequent compound design retained both fragments and investigated novel scaffolds to link the two, based on *in silico* predictions of SWIIP fit and considering only ligands preorganized in solution with a minimum energy conformation similar to the predicted bound conformation and with maximized diversity from known chemotypes. A dimethylpyrazole moiety appeared to satisfy all these criteria and was therefore selected for synthesis as **[3]**, which exists as a stable atropisomer due to hindrance of free rotation around the indazole–pyrazole bond by the presence of the two methyl substituents.

The cocrystal structure of **[3]** with KRAS^{G12C} confirmed the design hypothesis (Supplementary Fig. S1C). Initial SAR exploration aimed to decrease promiscuous cysteine chemical reactivity, being assessed by incubation of compounds with glutathione (28), versus specific (KRAS^{G12C}) reactivity. This resulted in replacement of the aniline linker by a spirocyclic azetidine moiety, as represented with **[4]** (Supplementary Table S1). Further molecular optimization of specific reactivity while maintaining the preorganized conformation of the single atropisomer ultimately resulted in the design and synthesis of JDQ443 **[5]** (Fig. 1A; Supplementary Table S1).

The crystal structure of JDQ443 bound to KRAS^{G12C} contained two monomers in the asymmetric unit. Figure 1B shows the binding mode of JDQ443 monomer 1 and its unique features. JDQ443 occupies the binding site in a distinct and novel way. The methyl-Cl indazole occupies a similar region as **[1]**, with the Cl and methyl substituents optimally filling the hydrophobic region delimited by V103, I100, M72, and Q99 (Cα and Cβ). The rigid spirocyclic linker (Fig. 1B) orients the acrylamide toward cysteine-12 and the amide carbonyl to form hydrogen bond interactions with the side chain of K16 and a water-mediated interaction with the Mg ion and the GDP beta phosphoryl group. The methyl indazole is slightly twisted out of the plane of the pyrazole core, allowing a sandwiched positioning of the indazole between the switch II loop and the side chain of Q99. In particular, it forms stacking interactions with the backbone amide of E63-Y64 and is in contact with the side-chain amide of Q99. Among published structures of KRAS^{G12C} inhibitors, these interactions are unique to JDQ443 binding, and JDQ443 is the first selective KRAS^{G12C} inhibitor with a 5-membered aromatic scaffold to enter clinical development. Of note, like sotorasib and in contrast to adagrasib, JDQ443 does not interact directly with H95 in monomer 1 (Supplementary Fig. S2A–S2C). With monomer 2 (Supplementary Fig. S3A and S3B), H95 points toward the ligand and forms Van der Waals contacts with the methyl–indazole moiety.

JDQ443 Potently Inhibits KRAS^{G12C} Cellular Signaling and Proliferation in a Mutant-Selective Manner

To elucidate the mode of action of JDQ443, assays were performed to characterize covalent bond formation with KRAS^{G12C} and the reversible binding affinity of the compound to the RAS wild-type (WT) paralogs. JDQ443 demonstrated covalent, irreversible KRAS^{G12C} binding and low reversible binding affinity to the RAS SWIIP in the GDP-bound state (Table 1). The mutant selectivity of JDQ443 translated in cellular systems, with JDQ443 potently and

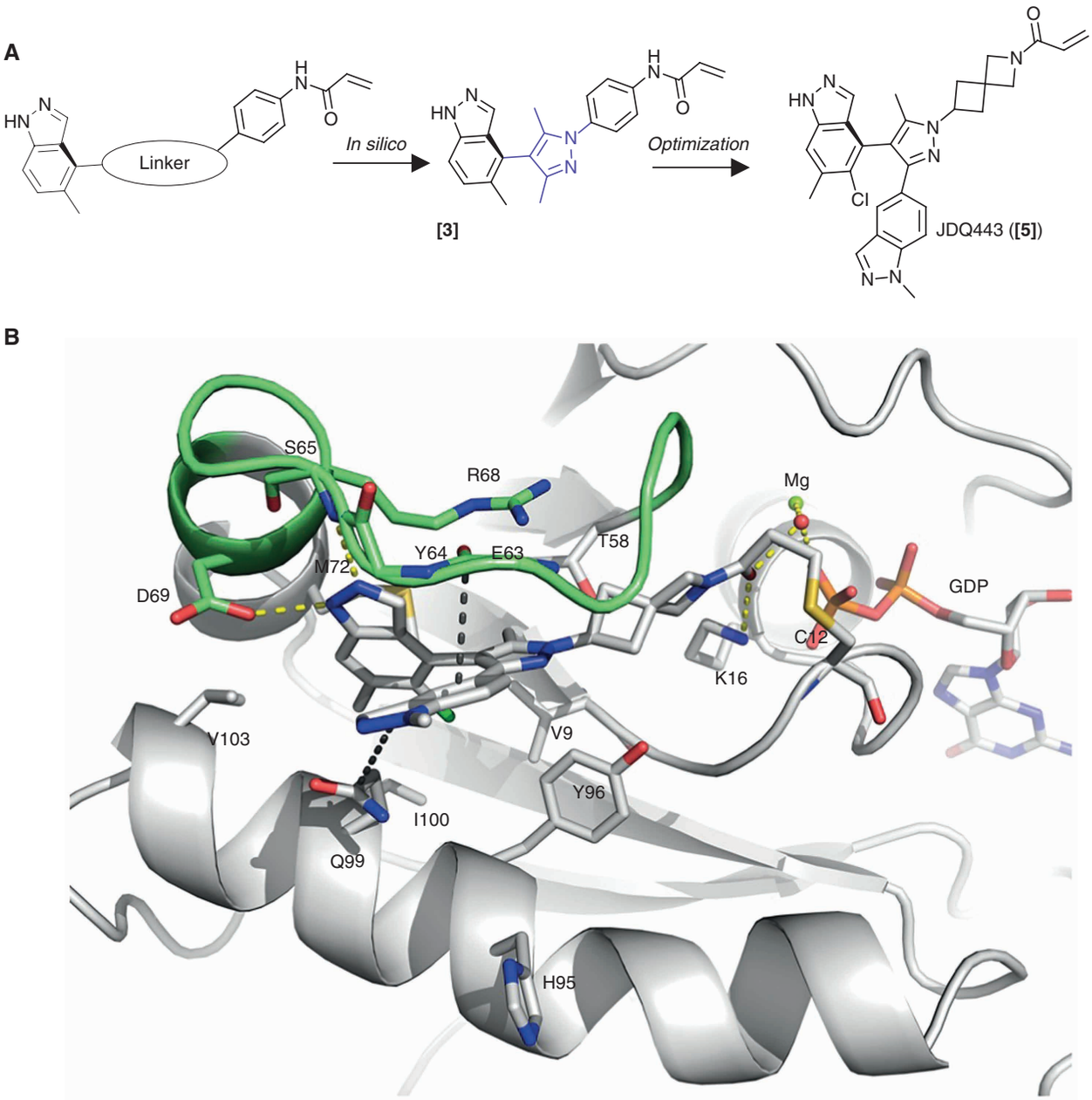

Figure 1. Design of JDQ443 and its binding mode to KRAS^{G12C}. **A,** Scheme of the design concept to maintain the indazole and the phenyl acrylamide pharmacophores and design a scaffold to link them. Several scaffolds were evaluated *in silico* and the best group (dimethyl pyrazole) selected for synthesis **[3]** and further optimized to give JDQ443 (**[5]**; see Supplementary Table S1). **B,** Crystal structure of JDQ443 monomer 1 in complex with KRAS^{G12C}. H-bonds are shown as yellow dotted lines. The indazole moiety forms H-bond interactions with the side chain of D69 and the backbone amide donor of S65 as well as fills the hydrophobic region delimited by V103, I100, M72, and Q99 (Cα and Cβ). The pyrazole is positioned at ~60° to the indazole fragment with the methyl pointing toward R68, T58, M72, and V9. In addition, it forms edge-to-face interactions with Y96. The spirocyclic group is a rigid linker optimally orienting the acrylamide toward C12 and the amide carbonyl to form hydrogen bond interactions with the side chain of K16 and water-mediated interaction to the Mg^{2+} ion and the beta phosphoryl group of GDP. The methyl-indazole moiety is almost planar to the pyrazole, and it is sandwiched between the switch II and the Q99 side chain (black dotted lines). Major differences between the two JDQ443 monomers are the conformation of H95 (pointing toward the ligand in monomer 2; Supplementary Fig. S3) and the interactions of the methyl-indazole moiety.

selectively inhibiting effector recruitment to KRAS^{G12C}, but not to RAS WT paralogs as demonstrated in the mechanistic KRAS:cRAF NanoBiT recruitment assay in HEK293 cells (Table 1). JDQ443 treatment promoted dose-dependent reductions of phosphorylated ERK (pERK) levels and the proliferation of the *KRAS*^{G12C}-mutated cell lines NCI-H358 and NCI-H2122, but not of the *KRAS-WT/MEK-Q56P* cell line NCI-H1437 (Table 1; Supplementary Fig. S4A–S4C). Comparative data for sotorasib and adagrasib are shown in Supplementary Table S2.

Table 1. JDQ443 covalently and selectively binds and inhibits GDP-bound KRAS^{G12C} with low reversible binding affinity to the RAS switch II pocket, and also inhibits proliferation of *KRAS*^{G12C}-mutated and *KRAS G12C/H95*, *G12C/R68S*, *and G12C/Y96* double-mutant cell lines

Biochemical assays Mean (SEM) [*n*] data		Cellular assays Mean (SD) data				
			pERK IC_{50} μmol/L (*n* = 3)		Proliferation GI_{50} μmol/L (*n* = 3)	
k_{inact}/K_I mmol/L^{-1}s^{-1}	K_D μmol/L	cRAF recruitment IC_{50} μmol/L (*n* = 3; HEK293)	NCI-H358/ NCI-H1437 (6 hours)	NCI-H2122/ NCI-H1437 (2 hours)	NCI-H358/ NCI-H1437 (3 days)	NCI-H2122/ NCI-H1437 (5 days)
141 (5.1) [34]	**GDP-bound:** • KRAS^{WT} 30.6 (3.5) [19] • NRAS^{WT} 26.6 (2.8) [18] • HRAS^{WT} 86.5 (10.8) [15] **GMPNP-bound:** • All >200	• KRAS^{G12C} 0.012 (0.0008) • KRAS^{WT} >1 • NRAS^{WT} >1 • HRAS^{WT} >1	• KRAS^{G12C} 0.018 (0.003) • RAS^{WT}MEK^{Q56P} >1	• KRAS^{G12C} 0.063 (0.004) • RAS^{WT}MEK^{Q56P} >1	• KRAS^{G12C} 0.019 (0.002) • RAS^{WT}MEK^{Q56P} 3.61 (0.49)	• KRAS^{G12C} 0.133 (0.013) • RAS^{WT}MEK^{Q56P} 4.54 (0.75)

Proliferation (GI_{50}) of *KRAS G12C* double mutants Mean (SD) μmol/L (Ba/F3 cells, *n* = 4)						
G12C	G12C/H95R	G12C/H95Q	G12C/H95D	G12C/R68S	G12C/Y96C	G12C/Y96D
0.115 (0.060)	0.024 (0.006)	0.284 (0.041)	0.612 (0.151)	>1	>1	>1

NOTE: The k_{inact}/K_I second-order rate constant determined by scintillation proximity assay (covalent competition); K_D by surface plasmon resonance; pERK by MesoScale Discovery assay; cRAF recruitment by NanoBiT PPI luminescence assay (Promega); and proliferation by CellTiter-Glo (Promega; NCI-H2122/NCI-H1437 and Ba/F3 *KRAS* mutants) or resazurin assay (NCI-H358/NCI-H1437). See Supplementary Methods for details. SD not assessed for results >1 μmol/L.

Abbreviation: GMPNP, guanyl-5′-yl imidodiphosphate.

In order to assess the breadth of mutant selectivity in a cellular setting, JDQ443 antiproliferative activity was assessed by a high-throughput cell viability assay in a large panel of *KRAS*^{G12C}-mutated (*N* = 17) and non–*G12C*-mutated (*N* = 225) cell lines from the Cancer Cell Line Encyclopedia (29). JDQ443 demonstrated potent antiproliferative activity selectively toward the *KRAS*^{G12C}-mutated lines (Fig. 2A and B).

To gain an understanding of the proteome-wide selectivity of JDQ443, we performed an LC/MS-based tandem mass tag proteomics experiment profiling the reactivity of over 11,500 cysteine-containing peptides, with NCI-H358 cells treated with 10 μmol/L JDQ443 or DMSO for 6 hours prior to enrichment of cysteine-containing peptides. We observed >2-fold competition of the peptide containing KRAS cysteine-12 (Fig. 2C) in JDQ443-treated versus DMSO-treated samples. Eight additional cysteine residues on six different proteins display a similar level of competition, indicating apparent labeling by JDQ443, the majority of which are frequently competed by unrelated electrophilic compounds screened in-house and in similar profiling efforts (30). Some of these are also competed by ARS-1620: HMOX2_C282 (31), VAT1_C50, VAT1_C86 (31), and FAM213A_C85 (17). Together, these results indicate that JDQ443 is highly selective across the proteome for the cysteine-12 residue of KRAS. Comparative data for sotorasib are shown in Supplementary Fig. S5.

To determine JDQ443 antiproliferative activity in the context of potential on-target resistance mutations, second-site mutants reported to confer resistance to adagrasib (22, 23) were engineered *in cis* with *KRAS*^{G12C} and expressed in Ba/F3 cells. The antiproliferative activity of JDQ443 in these cells versus those expressing *KRAS*^{G12C} alone was assessed via CellTiter-Glo cell viability assays. JDQ443 inhibited signaling and proliferation of the KRAS G12C/H95 double mutants G12C/H95R and G12C/H95Q (Table 1; Fig. 2D; Supplementary Fig. S6A), whereas expression of G12C/R68S, G12C/Y96C, and G12C/Y96D double mutants conferred resistance to JDQ443. These findings are in agreement with the binding mode described for monomer 1 and point to its relevance over monomer 2. Although JDQ443 does not interact directly with H95, expression of G12C/H95D resulted in reduced sensitivity to JDQ443 (Table 1). Western blot analysis of pERK upon JDQ443 treatment (Supplementary Fig. S6A) as well as the analysis of the rate constants of JDQ443 (Supplementary Table S3) toward these clinically observed SWIIP mutations in biophysical settings were in agreement with the cellular growth inhibition data (Table 1). The difference between H95D compared with H95R/Q could be due to the negative charge of the aspartate increasing the negative electrostatic potential of the KRAS^{G12C} surface, potentially affecting ligand recognition and decreasing JDQ443-specific KRAS^{G12C} reactivity and cellular activity. Another possible explanation is that the H95D mutation could affect KRAS structural dynamics so that the conformation allowing JDQ443 binding becomes less favored. Comparative data for sotorasib and

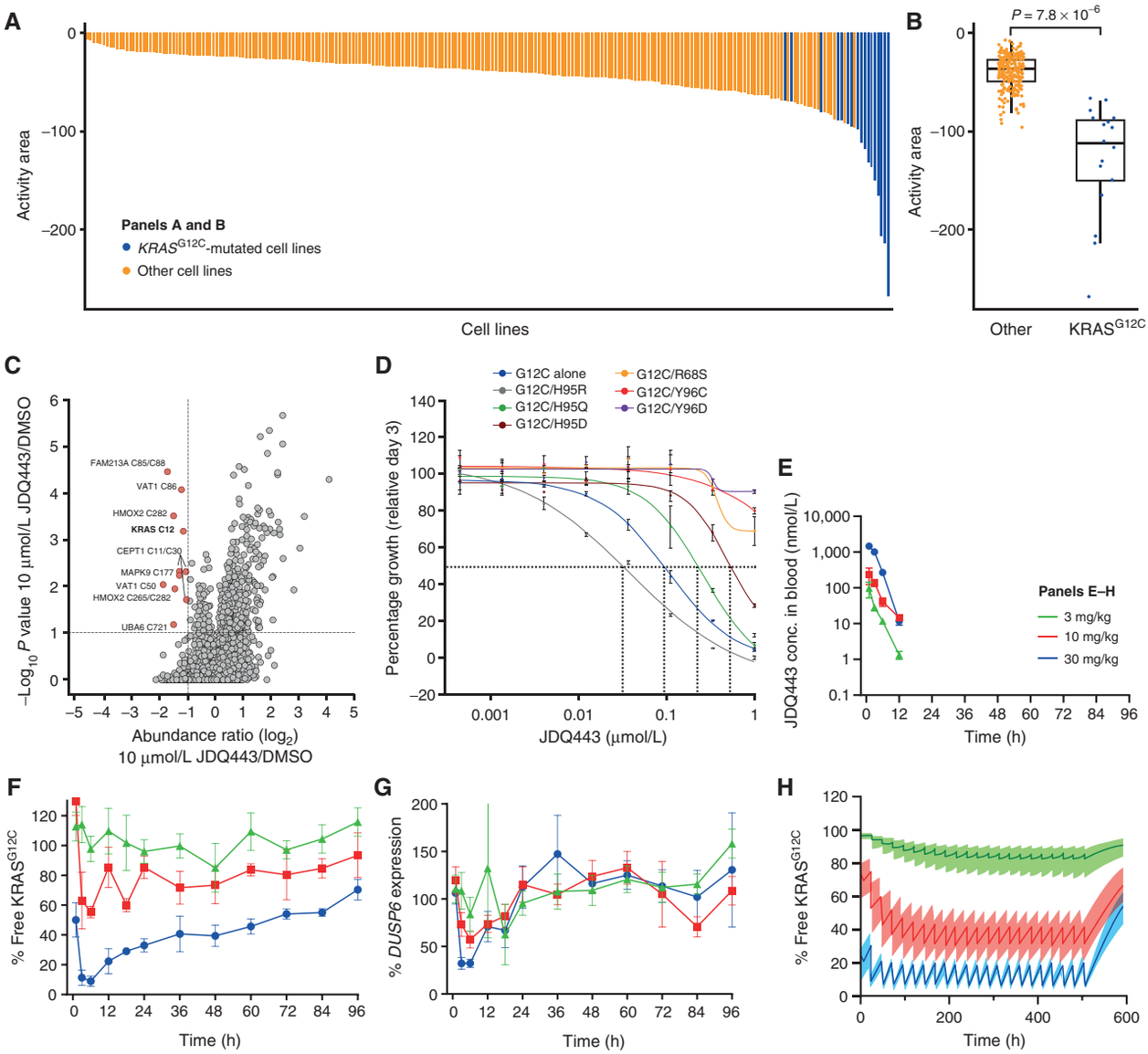

Figure 2. JDQ443 has selective activity for KRAS^{G12C}, including H95 double mutants, and shows dose-dependent single-dose pharmacokinetics and pharmacodynamics in mouse tumor models. **A,** Waterfall plot shows increased sensitivity to JDQ443 (activity area measuring the antiproliferative effect of JDQ443 relative to DMSO vehicle control over an 8-point dilution range) for 242 cancer cell line models included in this study. **B,** Cell lines were categorized by KRAS status (17 of 242 *KRAS*^{G12C} mutant); the distribution of their measured sensitivity to JDQ443 using activity area is represented in a box plot format, with the box extending from the 25th to 75th percentile with a line at the median and whiskers extending to the minimum and maximum values in each category. *P* value was calculated using a nonparametric unpaired *t* test. **C,** A profile of NCI-H358 cysteine reactivity with and without JDQ443 treatment (10 µmol/L, 6 hours). **D,** JDQ443 inhibits the proliferation of KRAS G12C/H95 double mutants. Ba/F3 cells expressing the indicated FLAG-KRAS^{G12C} single or double mutants were treated with the indicated concentrations of JDQ443 for 3 days, and the inhibition of proliferation was assessed by the CellTiter-Glo viability assay. The growth inhibition curves of one representative assay are shown. **E–G,** MIA PaCa-2 tumor-bearing nude mice were treated with a single oral dose of JDQ443 at indicated doses. Animals were sacrificed at multiple time points post-dose to collect blood and tumor samples to determine total drug concentrations in blood (**E**), LC-MS–based TO (free tumor KRAS^{G12C}; **F**), and tumor DUSP6 levels (**G**). Values are mean ± SD. conc., concentration. **H,** PK/PD model based on single-dose JDQ443 administration in MIA PaCa-2 xenografts predicts increased tumor KRAS^{G12C} inhibition over repeated dosing.

adagrasib are shown in Supplementary Tables S2 and S3 as well as Supplementary Fig. S6B and S6C.

JDQ443 Pharmacokinetics and Pharmacodynamics in Tumor-Bearing Nude Mice

The pharmacokinetic/pharmacodynamic (PK/PD) activity of JDQ443 was studied in the *KRAS*^{G12C}-mutated MIA PaCa-2 pancreatic and NCI-H2122 lung cancer cell–derived xenograft (CDX) mouse models. In a single ascending dose study, JDQ443 blood exposure increased with increasing doses up to 30 mg/kg (Fig. 2E) and from 30 to 100 mg/kg (Supplementary Fig. S7A). JDQ443 reached maximum concentration in blood ~1 to 2 hours after dosing and was rapidly eliminated from the systemic circulation, reflecting the short half-life

in mice ($T_{½}$ = 1.4–3.0 hours). Free tumor KRAS^{G12C} levels (noncovalently modified KRAS^{G12C}), a measure of target occupancy (TO), were robustly reduced in a dose-dependent manner (Fig. 2F; Supplementary Fig. S7B), and TO was sustained despite the PK short half-life, reflecting the covalent activity of JDQ443. Treatment-related reduction of free tumor KRAS^{G12C} correlated with suppression of the MAPK pathway target gene *DUSP6* (Fig. 2G; Supplementary Fig. S7C).

The relationship between the single-dose JDQ443 PK and TO in the MIA PaCa-2, NCI-H2122, and LU99 CDX models was characterized using a mathematical model (Supplementary Methods). This PK/TO model captures the inherent decoupling of kinetic timescales between drug PK (rapid) and TO (prolonged) that is observed across CDX models and allows for the estimation of a CDX-specific KRAS^{G12C} resynthesis rate. The simulations suggest that the KRAS^{G12C} resynthesis rate is a key parameter to understanding the PK/TO relationship. We estimated KRAS^{G12C} resynthesis half-lives and 95% confidence intervals (CI) of 83 hours (67–103 hours) in MIA PaCa-2, 21 hours (17–26 hours) in NCI-H2122, and 14 hours (10–18 hours) in LU99. The longer MIA PaCa-2 resynthesis half-life reflects its high sensitivity to KRAS^{G12C} inhibition. The slow resynthesis half-life in these tumor models facilitates sustained covalent TO despite the relatively short PK half-life of JDQ443 in mice. Simulated profiles suggest further decreases of free KRAS^{G12C} after repeated daily dosing (3, 10, 30 mg/kg), corresponding to greater sustained TO over time, in the MIA PaCa-2 (Fig. 2H), NCI-H2122 (Supplementary Fig. S7D), and LU99 (Supplementary Fig. S7E) CDX models.

JDQ443 Shows Antitumor Activity in *KRAS*^{G12C}-Mutated CDX Models, Driven by Daily AUC and TO

We assessed the single-agent antitumor activity of JDQ443 at daily oral doses of 10, 30, and 100 mg/kg in a panel of *KRAS*^{G12C}-mutated CDX models across different indications. Cell lines for xenografting were MIA PaCa-2 (PDAC); NCI-H2122, LU99, HCC44, NCI-H2030 (NSCLC); and KYSE410 (esophageal cancer). JDQ443 inhibited the growth of all models in a dose-dependent manner (Fig. 3A), with model-specific differences in dose-response dynamics and maximal response patterns that ranged from regression (MIA PaCa-2, LU99), to stasis (HCC44, NCI-H2122) to moderate tumor inhibition (NCI-H2030, KYSE410). The largest dynamic range was observed in LU99. In contrast, JDQ443 showed no growth inhibition in a KRAS^{G12V}-mutated xenograft model (NCI-H441; Fig. 3B), confirming KRAS^{G12C} specificity and consistent with the *in vitro* data. Efficacy was maintained across once-daily (q.d.) or twice-daily (b.i.d.) administration of the same daily dose: 30 mg/kg q.d. versus 15 mg/kg b.i.d. in MIA PaCa-2 (Fig. 3C), or 100 mg/kg q.d. versus 50 mg/kg b.i.d. in NCI-H2122 and LU99 (Fig. 3D and E). The efficacy of q.d. versus b.i.d. dosing correlated well with comparable daily area under the concentration–time curve (AUC) in blood (Supplementary Table S4). Comparative data for sotorasib and adagrasib are shown in Supplementary Fig. S8A–S8C.

These findings demonstrate that antitumor activity can be achieved under both q.d. and b.i.d. dosing. To better understand the relationship between PK, target occupancy, and efficacy, a continuous infusion xenograft study was performed in the LU99 xenograft model and the PK/TO model applied to estimate the resulting levels of KRAS^{G12C} target occupancy. Once-daily oral dosing at 30 mg/kg induced stasis for about 1 week followed by tumor progression, and 100 mg/kg induced tumor regression (Fig. 3F), with approximate steady-state average concentrations (C_{av}) of 0.3 and ~1 μmol/L, respectively. To assess continuous dosing, JDQ443 was delivered intravenously via programmable microinfusion pumps to achieve target concentrations approximating these oral C_{av} (Supplementary Table S5). Continuous infusion and oral dosing resulted in comparable antitumor responses (Fig. 3F and G). Further analysis of the antitumor responses and simulations of the PK/TO model demonstrate that efficacy correlates with both the daily AUC of JDQ443 and KRAS^{G12C} target occupancy (Fig. 3H and I) rather than other PK metrics, such as C_{max} and time over threshold (Supplementary Fig. S9A and S9B). Although the correlation of efficacy and TO was expected, given the nature of the covalent mode of inhibition, the correlation to daily exposure was unexpected and presents the opportunity to utilize JDQ443 AUC as a readily measurable surrogate for TO in preclinical and clinical studies.

Activity of JDQ443 Alone and in Combination in *KRAS*^{G12C}-Mutated NSCLC and Colorectal Cancer Patient-Derived Xenograft Models

We have previously demonstrated the clinical translatability of the large-scale *in vivo* patient-derived xenograft (PDX) model screening of drug candidates using the 1 × 1 × 1 mouse clinical trial (MCT) paradigm (32). Consequently, we evaluated the *in vivo* efficacy of JDQ443 at 100 mg/kg q.d. (single agent and in combination regimens) in an MCT study using representative PDX panels of *KRAS*^{G12C}-mutated NSCLC (Fig. 4A–D) and colorectal cancer (Fig. 4E–H; n = 9 each panel). The genetic alterations identified in each panel are detailed in Supplementary Table S6, though the sample size did not enable conclusive correlations between genetic comutations and efficacy. Single-agent JDQ443 demonstrated antitumor activity in both panels, with deeper responses in NSCLC than colorectal cancer (Fig. 4A vs. 4E; Supplementary Table S7), consistent with reported clinical findings for other single-agent KRAS^{G12C} inhibitors in these indications (20, 21, 25, 33).

Inhibitors of SHP2 may have the potential to synergize with JDQ443. Inhibition of SHP2 impedes the growth of *KRAS*-mutant cancer cell lines in part by shifting the pool of KRAS to the inactive GDP-loaded state (34–36). As JDQ443 binds exclusively to GDP-bound KRAS^{G12C}, combined SHP2 and KRAS^{G12C} inhibition is predicted to be synergistic due to the increased target pool for irreversible JDQ443 binding.

To evaluate the concept of combining JDQ443 with the SHP2 inhibitor TNO155 (37) *in vitro*, a panel of *KRAS*^{G12C}-mutated NSCLC cell lines was treated with each compound alone or concomitantly (37) for 6 and 24 hours. Cotreatment resulted in JDQ443 concentration-dependent reduction in both ERK and RSK3 phosphorylation (Supplementary Fig. S10A and S10B) and *DUSP6* gene expression (Supplementary Fig. S10C), which were more pronounced than with JDQ443 alone. We then tested the combination of JDQ443 with TNO155 in 7-day viability assays on a panel of *KRAS*^{G12C}-mutated NSCLC cell lines. Cells were treated with increasing

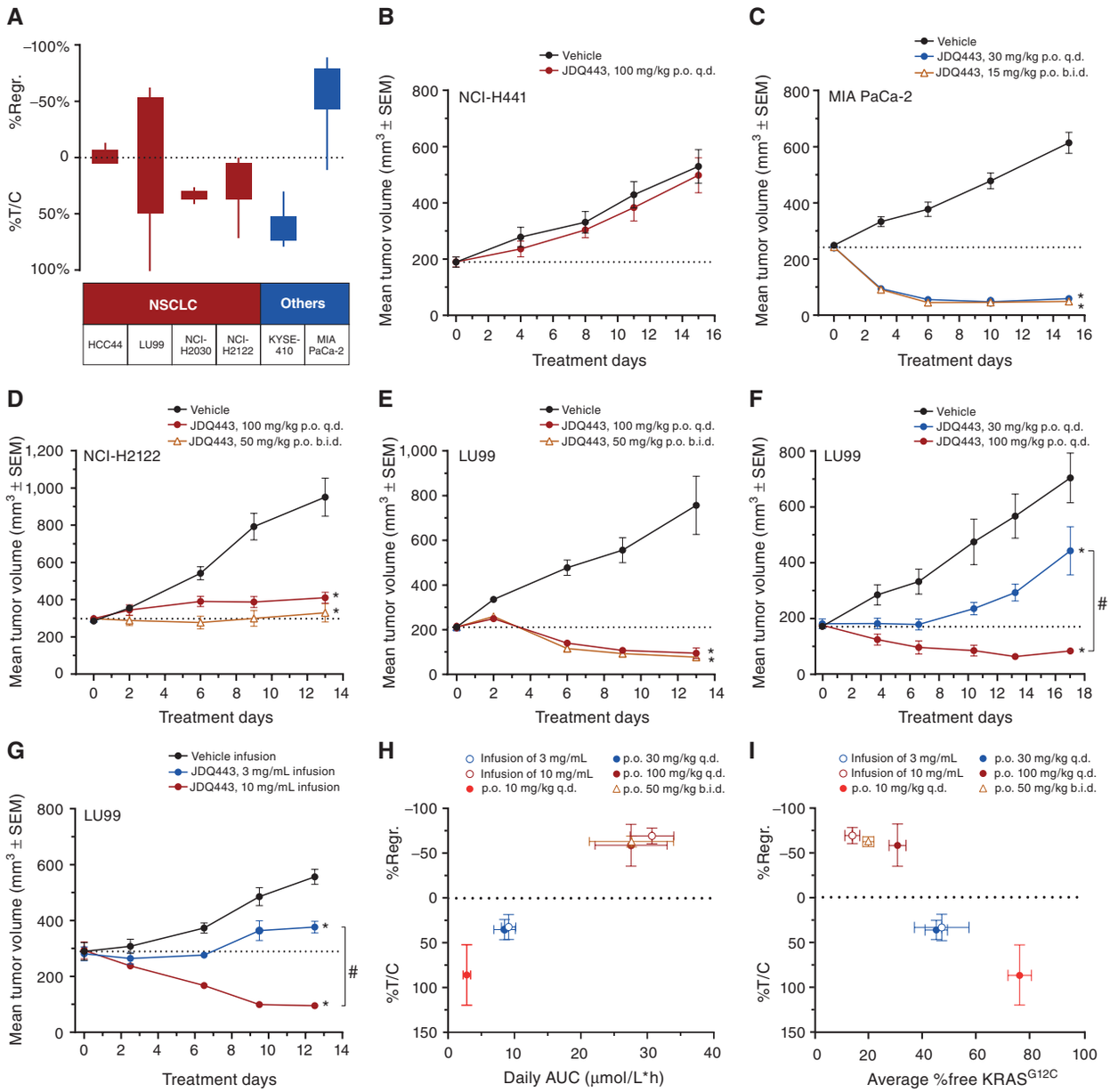

Figure 3. JDQ443 displays antitumor activity across a range of cell-derived, *KRAS*^{G12C}-dependent mouse tumor models, with efficacy driven by daily AUC. **A,** Aggregated best tumor growth inhibition in six KRAS^{G12C} tumor models. JDQ443 efficacy was evaluated after oral dosing of 10, 30, and 100 mg/kg/day in six human *KRAS*^{G12C}-mutant CDX models in mice. NSCLC cell line models are depicted in red, whereas PDAC (MIA Paca-2) and esophageal (KYSE410) cancer cell line models are shown in blue. Data are means from 2–11 independent *in vivo* studies. %Regr. is percentage tumor volume regression [−(Δtreated/treated at baseline) × 100], and %T/C is percentage tumor volume growth ratio [(Δtreated/Δcontrol) × 100]. **B–G,** CDX-bearing mice with *KRAS*^{G12C}-mutated (**C**–**G**) and non-G12C-mutated (NCI-441, KRAS^{G12V}; **B**) tumors were treated orally (p.o.) with JDQ443 at the indicated doses and schedules. **G,** LU99 tumor–bearing mice were treated with JDQ443 by continuous intravenous infusion using a programmable microinfusion pump. **H** and **I,** Simulated population-PK/PD metrics of daily AUC of JDQ443 in mouse blood (**H**) and average free KRAS^{G12C} levels in tumor at steady state (**I**) are correlated with the observed efficacy in LU99 (%T/C or % regression). Points correspond to the mean and the error bars to ± 1 SD of the simulated PK/PD metrics based on 100 simulations and observed efficacy metrics. *, $P < 0.05$ versus vehicle; #, $P < 0.05$ versus each other, by one-way ANOVA.

JDQ443 concentrations with or without TNO155. In most cell lines, the combination led to greater cell growth inhibition or cell killing compared with single-agent JDQ443. Limited to no combination benefit was observed in NCI-H2030, HCC44, and LU99 cell lines at those concentrations (Supplementary Fig. S10D). Comparative growth inhibition matrices across a panel of *KRAS*^{G12C}-mutated cell lines for JDQ443, sotorasib, and adagrasib in combination with TNO155 or trametinib are shown in Supplementary Fig. S10E and S10F.

Blockade of SHP2 or MEK1/2 may disrupt RAS pathway reactivation typically observed upon prolonged KRAS^{G12C} inhibition (38). Therefore, we evaluated whether combining

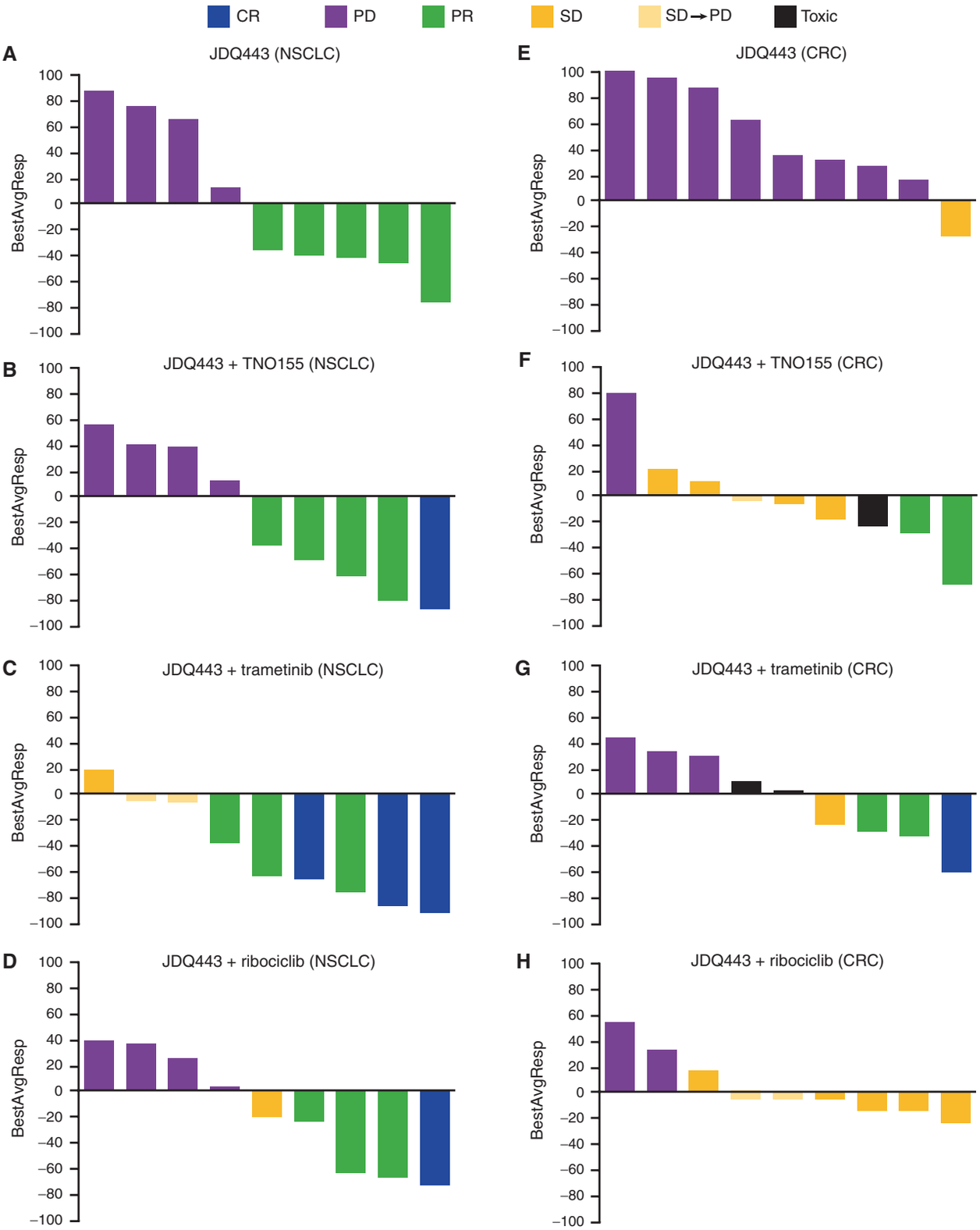

Figure 4. JDQ443 generates categorical antitumor responses in PDX models of NSCLC and colorectal tumors that are improved by combination treatment with other agents. Nude mice bearing *KRAS*^{G12C}-mutated NSCLC (**A**–**D**) and colorectal cancer (CRC; **E**–**H**) PDX models were treated with daily oral doses of JDQ443 at 100 mg/kg or with JDQ443 in combination with TNO155 (10 mg/kg p.o. b.i.d.), trametinib (0.3 mg/kg p.o. q.d.), or ribociclib (75 mg/kg p.o. q.d.) in a 1 × 1 × 1 format (1 mouse × 1 model × 1 treatment). Best average responses (BestAvgResp) are shown, with response categories adapted from RECIST criteria (see Methods for details). CR, complete response; PD, progressive disease; PR, partial response; SD, stable disease.

JDQ443 with TNO155 or trametinib improves JDQ443 single-agent activity in our *in vivo* PDX panels. In both NSCLC and colorectal cancer panels, combination with either compound improved JDQ443 single-agent responses (Fig. 4A–C and E–G; Supplementary Table S7). In addition, JDQ443 single-agent extension of tumor doubling time versus untreated mice, another measure of efficacy in an MCT, was also further extended by both combinations (Supplementary Fig. S11A and S11B).

Finally, KRAS is a known regulator of cyclin D proteins, regulating cell proliferation by triggering RB/E2F-dependent entry into the cell cycle. In a subset of *KRAS*^{G12C}-mutated NSCLC, *CDKN2A* (p16) mutations coincide and hyperactivate CDK4/6-dependent RB phosphorylation and cell-cycle transition, suggesting increased dependence on CDK4/6 activity in these tumors. Previous studies have reported a synthetic lethal interaction between KRAS and CDK4 in a mouse model of NSCLC (39, 40). Therefore, we studied JDQ443 in combination with the CDK4/6 inhibitor ribociclib. Similar to TNO155 and trametinib, ribociclib improves JDQ443 single-agent activity in both NSCLC and colorectal cancer PDX panels (Fig. 4A, D, E, and H; Supplementary Table S7) and extends the tumor doubling time versus untreated mice (Supplementary Fig. S11A and S11B).

Collectively, these data demonstrate the broad antitumor activity of JDQ443 in *KRAS*^{G12C}-mutated cancers and support the hypothesis that combination with TNO155, trametinib, or ribociclib can improve single-agent activity in *KRAS*^{G12C}-mutated NSCLC and colorectal cancer.

JDQ443 plus TNO155 Improves the Single-Agent Activity of JDQ443 in CDX Models, with Efficacy Maintained at Lower Doses of Either Drug

We further investigated the improved antitumor effect of JDQ443 in combination with TNO155 using different dose regimens in CDX models. JDQ443 at 100 mg/kg q.d. plus TNO155 at 7.5 mg/kg b.i.d. in three *KRAS*^{G12C}-mutated CDX models (LU99, NCI-H2030, and KYSE410) showed either greater tumor efficacy compared with each agent alone (H2030, KYSE410) or a delayed time to tumor progression (LU99; Fig. 5A–C). Furthermore, TNO155 at a reduced dose of 7.5 mg/kg q.d. (instead of b.i.d.) was sufficient to maintain efficacy with JDQ443 at 100 mg/kg q.d. in the LU99 and KYSE410 models (Fig. 5A–C). Next, we tested the effect of a JDQ443 dose reduction in combination with TNO155 in LU99, HCC44, and KYSE410 xenografts. In the LU99 model (Fig. 5D), JDQ443 at 30 mg/kg q.d. plus TNO155 at 7.5 mg/kg b.i.d. achieved the same response as single-agent JDQ443 at 100 mg/kg q.d. Similarly, in the HCC44 model (Fig. 5E), JDQ443 at 30 mg/kg q.d. plus TNO155 at 7.5 mg/kg b.i.d. achieved the same response as single-agent JDQ443 at 100 mg/kg. In KYSE410 (Fig. 5F), the combination of JDQ443 at 30 mg/kg q.d. plus TNO155 at 7.5 mg/kg b.i.d. was sufficient to achieve tumor stasis, whereas single-agent JDQ443 at 100 mg/kg q.d. had no significant effect. However, JDQ443 at 100 mg/kg q.d. plus TNO155 at 7.5 mg/kg b.i.d. further improved efficacy and caused tumor regression. The similar efficacy of JDQ443 30 mg/kg in combination with TNO155 and of JDQ443 100 mg/kg given alone in the LU99 model (Fig. 5D) was observed to correlate with TO. After 5 days of treatment, both the 100 mg/kg single-agent dose and the 30 mg/kg dose in combination with TNO155 achieved comparable reductions of free KRAS^{G12C} in LU99 tumors (Fig. 5G). However, one treatment of JDQ443 as a single agent at 30 mg/kg achieved less reduction of tumor KRAS^{G12C} than did 100 mg/kg (Fig. 5H), consistent with its dose-dependent, single-agent antitumor activity (Fig. 5D).

Together, these data indicate that SHP2 blockade by TNO155 can augment the antitumor activity of JDQ443 through enhancing TO to establish a deeper blockade of KRAS-dependent signaling, and that efficacy can be maintained even at a reduced exposure of either of the two drugs.

Evidence of JDQ443 and JDQ443 plus TNO155 Clinical Activity

A first-in-human clinical trial of JDQ443 (KontRASt-01 and NCT04699188) opened to enrollment in February 2021 to assess the safety, tolerability, and efficacy of JDQ443 alone or in combination with TNO155 and/or tislelizumab in patients with *KRAS*^{G12C}-mutated solid tumors. Two cases of patients treated in this trial are provided here to illustrate the clinical antitumor activity of JDQ443 alone or with TNO155 (Fig. 6).

Case 1: A 57-year-old male with metastatic *KRAS*^{G12C}-mutated NSCLC. Local molecular testing identified no mutations in *TP53*. Mutation status of *STK11*, *KEAP1*, and *NRF2* was unknown. The patient had received prior carboplatin/pemetrexed/pembrolizumab, docetaxel, tegafur–gimeracil–oteracil, and carboplatin/paclitaxel/atezolizumab. He was enrolled to the JDQ443 monotherapy dose-escalation part of the study at a dose of 200 mg JDQ443 b.i.d. given continuously on a 21-day cycle. Disease assessment after 2 cycles of treatment demonstrated a RECIST 1.1 partial response, with a –30.4% change in the sum of the longest diameters of target lesions compared with baseline. Partial response was confirmed on subsequent scans (Fig. 6), and the patient continued on treatment. Positron emission tomography imaging at baseline and after 4 cycles of treatment also showed substantial reduction in fluorodeoxyglucose (FDG) avidity of the tumor mass (Fig. 6).

Case 2: A 58-year-old female with *KRAS*^{G12C}-mutated duodenal papillary cancer metastatic to liver. An *R175H* mutation in *TP53* was observed by next-generation sequencing (FoundationOne panel). The patient had received prior treatment with cisplatin/gemcitabine and tegafur, each with a best response of progressive disease. She was enrolled to the dose-escalation portion of the study's JDQ443 + TNO155 arm, and received JDQ443 200 mg q.d. continuously with TNO155 20 mg q.d. 2 weeks on/1 week off. Disease assessment after two cycles of treatment demonstrated a RECIST 1.1 partial response (Fig. 6), with a –44.2% change in the sum of the longest diameters of target lesions compared with baseline. Partial response was confirmed on subsequent scans, and the patient continued on treatment.

DISCUSSION

We have described the discovery and characterization of JDQ443, an orally available, potent, selective, irreversible covalent inhibitor of GDP-bound KRAS^{G12C}, which is structurally

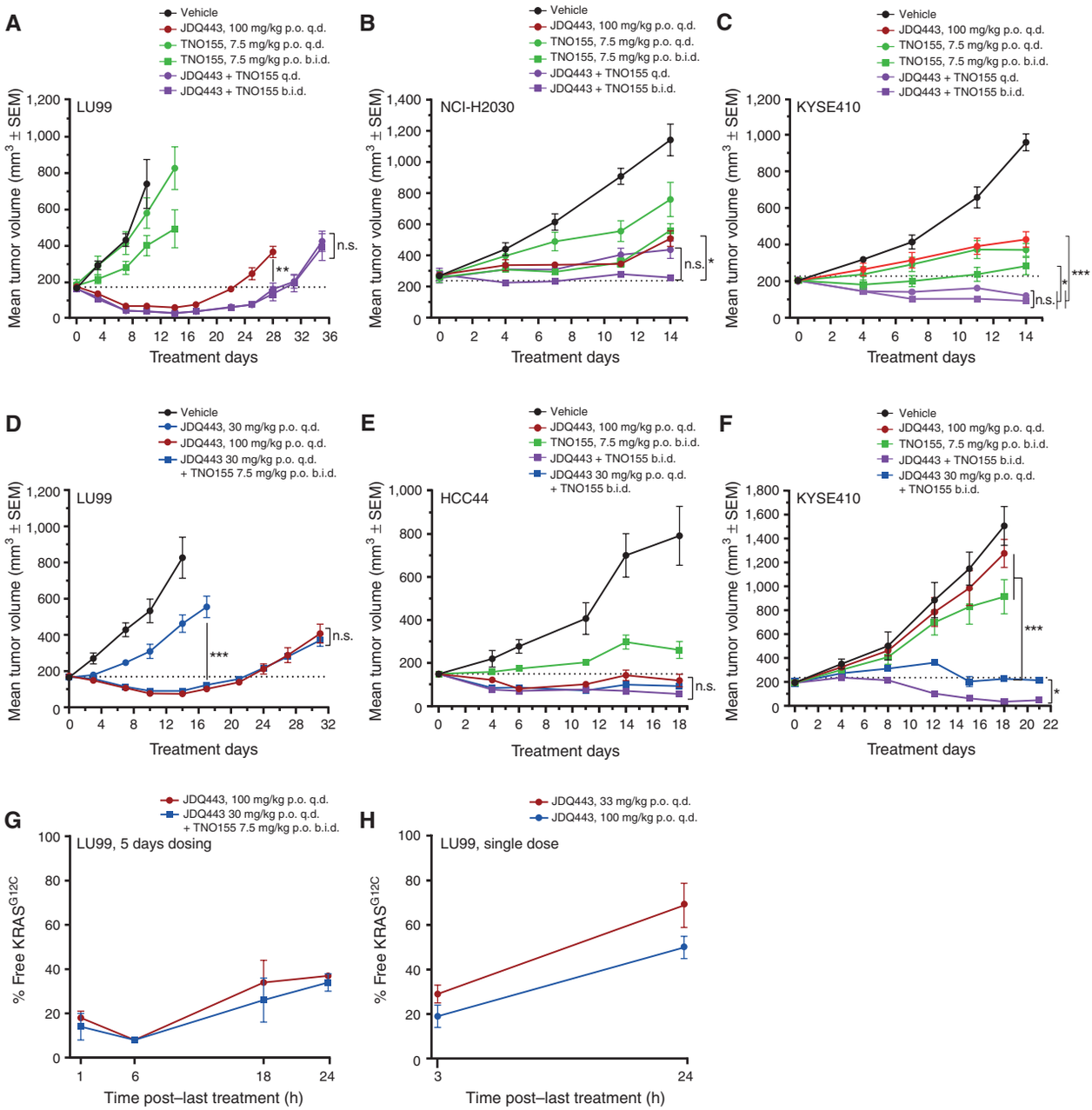

Figure 5. JDQ443 plus TNO155 improves the single-agent activity of JDQ443 in CDX models, with efficacy maintained with lower doses of either drug. **A–F,** CDX-bearing mice were treated orally (p.o.) with JDQ443, TNO155, or the combination thereof at the indicated doses and schedules. **G,** LU99 tumor–bearing nude mice were treated orally with JDQ443 alone or in combination with TNO155 at the indicated doses and schedules for 5 days. Tumors were taken at the indicated time points post–last dose, and free tumor $KRAS^{G12C}$ was determined. **H,** LU99 tumor–bearing nude mice were treated orally with JDQ443 at the indicated doses once. Tumors were taken at 3 and 24 hours after dose, and free tumor $KRAS^{G12C}$ was determined. Unless otherwise indicated, JDQ443 was dosed at 100 mg/kg p.o. q.d. and TNO155 at 7.5 mg/kg p.o. Data represent mean ± SEM; *, $P < 0.05$; **, $P < 0.01$; ***, $P < 0.001$; n.s., not significant (two-way ANOVA with Tukey multiple comparison test).

unique and exhibits a novel binding mode. JDQ443 shows early signs of clinical efficacy in patients with *KRAS*^{G12C}-mutated tumors, both as monotherapy and in combination with the SHP2 inhibitor TNO155.

The discovery of JDQ443 was based on the identification and optimization of a new $KRAS^{G12C}$ chemotype identified by structure-based *de novo* design. Analysis of published and in-house cocrystal structures suggested two key pharmacophoric features to be important for effective binding to the $KRAS^{G12C}$ SWIIP (methyl indazole and phenyl acrylamide). A new chemotype was discovered by retaining these two features and designing a linker that would maximize the diversity to known chemotypes while minimizing ligand flexibility. This latter consideration was based on the fact that the switch I and II

Case	Treatment	T_{max} (h)	C_{max} (ng/mL)	$AUC_{0–24\ h}$ (h*ng/mL)
1	JDQ443 200 mg b.i.d. continuously	7.8	5,920	75,930
2	JDQ443 200 mg q.d. continuously + TNO155 20 mg q.d. 2 weeks on/1 week off	3.2	5,270	55,670

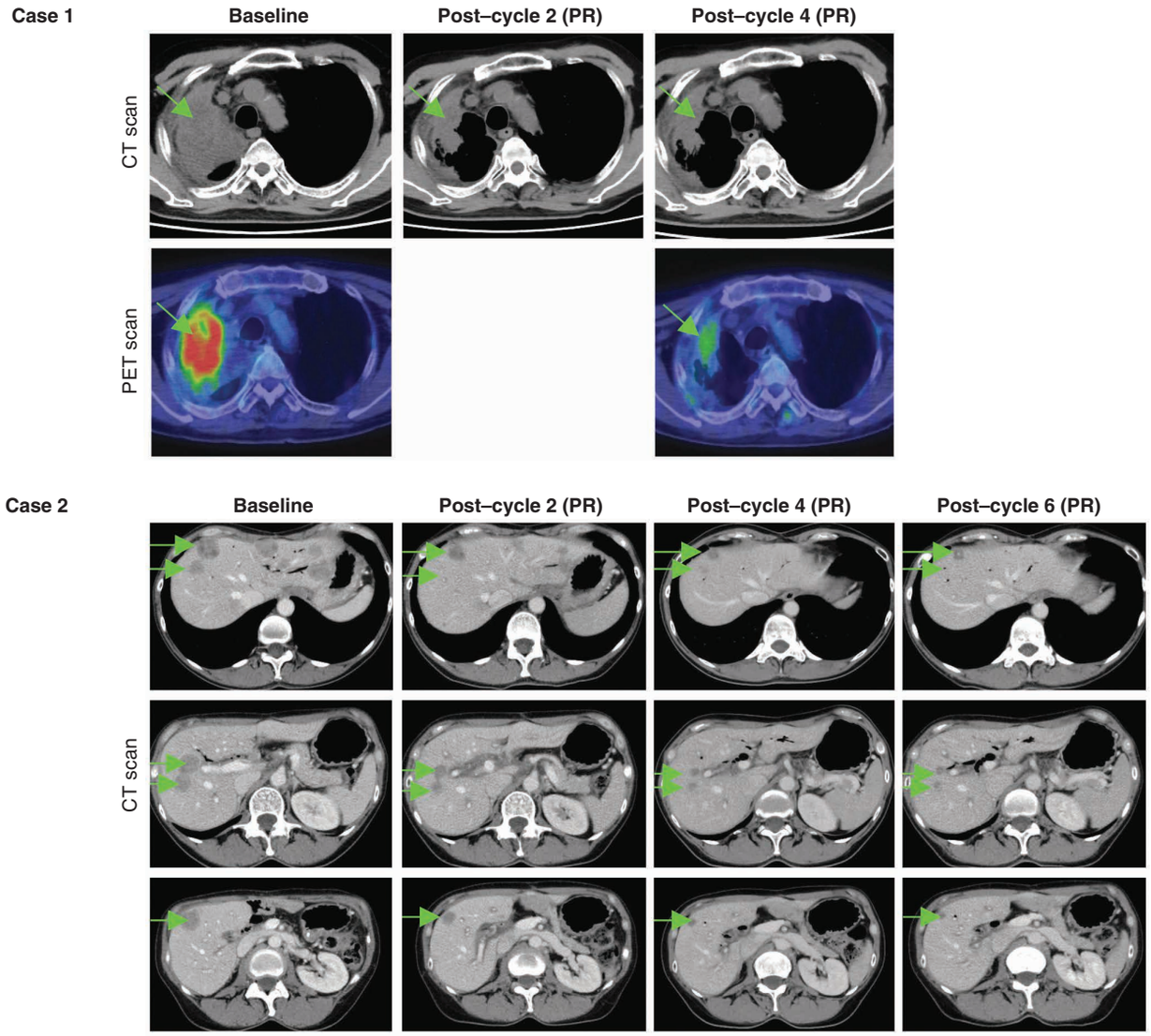

Figure 6. Serial axial CT/PET images and steady-state (cycle 1, day 14) JDQ443 PK parameters for clinical cases 1 and 2. Green arrows indicate locations of tumors. PR, partial response (RECIST 1.1 by local review).

regions of KRAS are highly flexible, with cocrystal structures of KRAS with either GDP or nonhydrolysable forms of GTP not showing any visible binding pocket besides the nucleotide-binding site. In solution, there might be many protein conformations with higher free energy where binding sites such as the SWIIP may exist. As a result, the preorganized conformation of JDQ443 in solution, similar to that of the bound molecule, reduces the ligand-free energy penalty and therefore maximizes its potential ability to bind to such higher free energy protein conformations. This is a common feature in the $KRAS^{G12C}$ ligand landscape and could potentially be broadly applied to the design of compounds targeting flexible proteins and/or allosteric pockets.

JDQ443 binds to the $KRAS^{G12C}$ SWIIP in a distinct way from sotorasib and adagrasib, occupying different regions of the pocket and exploiting new interactions. It is also the only potent $KRAS^{G12C}$ inhibitor currently described in the literature with a 5-membered aromatic scaffold, able to

optimally react with cysteine-12 via a rigid spirocyclic linker. These unique features may result in distinct resistance and/or tolerability profiles that may have implications for its combination use. In preclinical settings, JDQ443, sotorasib, and adagrasib show overall comparable profiles with one notable exception being their interactions with H95. All three compounds are in clinical development, and the most relevant comparisons between them will come from their respective clinical activities and their unique potential for combination strategies.

Resistance mechanisms to KRAS^{G12C} inhibitors that have been identified so far include *KRAS* amplification and on-target mutations in KRAS (including second-site mutations of KRAS^{G12C}); mutations in pathway components that are upstream (EGFR, RET, and FGFR2), in parallel (NRAS, NF1), or downstream (BRAF, MAP2K, PIK3CA, PTEN, and MYC) of KRAS activity; *MET* gene amplifications; acquired gene fusions; and mutations in other genes (22–24, 41–43). A non-uniform adaptive resistance process has also been reported, where the equilibrium of resynthesized KRAS^{G12C} in ARS-1620–treated subpopulations was quickly shifted toward the ON state due to upstream RTK activation reducing target engagement of the OFF state inhibitor (44).

Second-site mutations within the SWIIP show distinct sensitivity to adagrasib versus sotorasib depending on the binding mode of the inhibitor (42). KRAS^{G12C} second-site mutants H95R/Q/D mediate resistance to adagrasib but not to sotorasib, whereas Y96C/D and R68S significantly reduce the binding affinity and inhibitory potential of both drugs. In contrast to adagrasib and similarly to sotorasib, JDQ443 does not directly interact with H95. Consistent with this, JDQ443 potently inhibits the proliferation and signaling of G12C/H95 double mutants expressed in Ba/F3 cells. We speculate that JDQ443 may also prevent the clinical emergence of G12C/H95 resistance and could potentially overcome G12C/H95 resistance following prior adagrasib treatment. The heterogeneous mechanisms of KRAS^{G12C}-inhibitor resistance point to the biological ease and need to reactivate the driver oncogene and downstream MAPK pathway. Several groups have reported that resistance clones are not preexisting but occur via epigenetic adaptation of drug-tolerant persisters whereby some undergo further evolution to acquire genetic resistance mechanisms (45–47). This complex diversity of resistance patterns and their emergence will likely remain a challenge for all KRAS^{G12C} inhibitors used as single agents, and upfront maximal inhibition of the oncogenic driver or driver pathways with a strong combination strategy may therefore be the best approach to improve the durability of clinical response.

Previous studies demonstrating an elevated pool of GDP-bound KRAS^{G12C} under SHP2 inhibition (38, 48) provide a rationale for combining JDQ443 and the SHP2 inhibitor TNO155. We observed that this combination improved the single-agent activity of JDQ443, promoting increased TO of KRAS^{G12C}, greater suppression of oncogenic MAPK signaling, and delayed tumor regrowth in the LU99 model *in vivo* (Fig. 5). Another major determinant of KRAS^{G12C} inhibitor resistance is the reactivation of upstream tyrosine kinase signaling that promotes SOS1-dependent GTP loading on RAS family members (19, 38, 44, 48–50). Blocking critical resistant nodes upstream of SOS1, such as SHP2, could also result in a viable strategy to block the heterogeneous RTK families involved in MAPK signal reactivation. We observed that in the KYSE410 model, which mediates KRAS^{G12C} inhibitor resistance through *HER2* amplification, the combination of JDQ443 and TNO155 restored suppression of oncogenic MAPK signaling and induced tumor regression *in vivo* (Fig. 5).

Collectively, these data support combining JDQ443 and TNO155 to induce deeper and more durable responses in patients with *KRAS*^{G12C}-mutated tumors. Additionally, our observation that combination efficacy can be maintained in *in vivo* models at reduced exposures of either of the two drugs suggests the potential for flexibility in mitigating potential adverse events by dose reductions without compromising efficacy. Our data also support combining JDQ443 with the MEK inhibitor trametinib or the CDK4/6 inhibitor ribociclib. Given the diversity of KRAS^{G12C}-inhibitor resistance, an improved understanding of potential resistance pathways based on tumor type and/or baseline molecular characteristics may ultimately enable a more personalized approach to combination therapy that will require the development of multiple combinations.

The irreversible covalent nature of JDQ443 binding affects its PK/PD relationships and as a result facilitates minimizing clinical dosing needed to achieve a maximal response with the fewest adverse events. Consistent with covalent modification, KRAS^{G12C} TO by JDQ443 was sustained in preclinical CDX models despite its short PK half-life in mice. Daily dose splitting, infusion studies, and modeling suggest that the preclinical efficacy of JDQ443 is driven by systemic daily AUC, implying that although TO is a relevant biomarker, the daily AUC of JDQ443 can be used as a readily quantifiable surrogate of efficacy for clinical dose optimization.

JDQ443 is currently in clinical development as a monotherapy and in combination with either TNO155, the anti–PD-1 monoclonal antibody tislelizumab, or both (NCT04699188; ref. 51). We have highlighted two clinical cases showing antitumor activity of JDQ443 as monotherapy (case 1) in a patient with advanced NSCLC and in combination with TNO155 (case 2) in a patient with advanced duodenal cancer. This second case is particularly notable given that this patient had not benefited from prior chemotherapy, consistent with historical evidence of minimal chemotherapeutic efficacy in cases of unresectable advanced/metastatic small bowel adenocarcinoma (52). The combination of JDQ443 and TNO155 showed robust antitumor activity in this patient, despite JDQ443 in the combination being given at half the daily dose (200 mg q.d.) of the patient with NSCLC (case 1) who received JDQ443 monotherapy (200 mg b.i.d.). This result suggests that JDQ443 plus TNO155 may offer impactful clinical activity in *KRAS*^{G12C}-mutated populations previously refractory to standard treatments and, extrapolating from colorectal cancer data, in indications where single-agent KRAS^{G12C} inhibition has limited efficacy. Given the dependence on EGFR-mediated signaling in colonic tumors (50), the combination of KRAS^{G12C} inhibition with SHP2 inhibition may be particularly beneficial in these tumor types, similar to a KRAS^{G12C} inhibitor/EGFR inhibitor combination

(25) though with the added benefit of suppression of other RTK-mediated pathways.

Further data on JDQ443 monotherapy and the JDQ443 plus TNO155 combination in patients with *KRAS*^{G12C}-mutated tumors are forthcoming, and a randomized study comparing the activity of JDQ443 with standard-of-care docetaxel in previously treated locally advanced or metastatic *KRAS*^{G12C}-mutated NSCLC is planned (NCT05132075; KontRASt-02).

METHODS

JDQ443, TNO155, trametinib, ribociclib, sotorasib, and adagrasib were obtained from the Global Discovery Chemistry department at Novartis AG. All cancer cell lines, as well as the parental cell line HEK293 A used to generate the NanoBiT selectivity panel, were obtained from ATCC or DSMZ and are part of the Novartis Cancer Cell Line Encyclopedia (CCLE), validated as previously described (29). Cells were in culture for 8 to 12 weeks when running in flowchart assays. Cells were sporadically tested for *Mycoplasma* using the PCR Mycoplasma Test Kit I/C (PromoKine; #PK-CA91-1096) or the MycoAlert Mycoplasma Detection Kit (#LT07-218) from Lonza. The Ba/F3 parental cells were obtained from the Dana-Farber Cancer Institute in 2003. Cells were tested *Mycoplasma*-negative, and a large stock was produced at passage 3 for further use. Ba/F3 cells transduced with the indicated KRAS mutants have reached passage 8 after IL3 withdrawal and were used for a maximal 8 to 10 more passages for subsequent GI_{50} or Western blot analysis. *Mycoplasma* testing was not performed. Cells were maintained at 37°C in 5% CO_2 and cultured in DMEM high glucose (BioConcept Ltd. Amimed, #1-26F01-I), 10% FCS, 4 mmol/L L-glutamine, 1 mmol/L sodium pyruvate (MIA PaCa-2) and RPMI 1640 (BioConcept Ltd. Amimed, #2-01F30-I), 10% FCS (BioConcept Ltd. Amimed, #2-01F30), 2 mmol/L L-glutamine (BioConcept Ltd. Amimed, #5-10K00-H), 1 mmol/L sodium pyruvate (BioConcept Ltd. Amimed, #5-60F00-H), and 10 mmol/L HEPES (LU99, NCI-H2122, NCI-H2030, HCC44, KYSE410, and NCI-H441). Cell lines used for *in vivo* studies were confirmed *Mycoplasma*-free and pathogen-free (IMPACT-8; IDEXX BioAnalytics). For *in vivo* injection, cells were used between 5 and 12 passages after thawing. Genomics data for CCLE cell lines as published previously (53) were downloaded in November 2021 from www.cbioportal.org (54, 55).

In Vivo *CDX Studies*

Xenograft studies were performed at Novartis and strictly adhered to Novartis Institutes for BioMedical Research Animal Care and Use Committee protocols and regulations. Studies were approved by the Cantonal Veterinary Office of Basel Stadt, Switzerland, and in strict adherence to the Swiss Federal Animal Welfare Act and Ordinance, or by the U.S. Institutional Animal Care and Use Committee and were conducted in accordance with the guidelines published in the U.S. Guide for the Care and Use of Laboratory Animals. Mice were kept under optimal hygiene conditions in individually ventilated cages under 12-hour dark/12-hour light conditions and had access to sterilized food and water *ad libitum*. Subcutaneous tumors were induced by injecting cells in HBSS containing 50% BD matrigel in the flank of female athymic Crl:NU(NCr)-*Foxn1*^{nu}-homozygous nude mice (Charles River; MIA PaCa-2, NCI-H2122, NCI-H441 5×10^6; LU99 2×10^6) or female CB17.Cg-*Prkdc*^{scid}*Lyst*$^{bg\text{-}J}$ mice (Charles River; KYSE410 10×10^6). Subcutaneous NCI-H2030 and HCC44 tumors were induced by transplantation of tumor fragments in the flank of female C.B-*Igh*-1b/GbmsTac-*Prkdc*^{scid}-*Lyst*^{bg} N7 mice (Taconic).

For efficacy studies, treatment was started when the average tumor size had reached approximately 200 to 300 mm^3. Tumor size was measured twice weekly by caliper, and body weights were recorded twice weekly. Tumor size, in mm^3, was calculated using the formula (length × width^2) × $\pi/6$. Data are presented as mean ± SEM. As a measure of efficacy, the %T/C value was calculated at the end of the experiment using the formula (Δtumor volume^{treated}/Δtumor volume^{control}) × 100. In the case of tumor regression, the tumor response (%Reg) was quantified using the formula –(Δtumor volume^{treated}/tumor volume^{treated} at start) × 100. Statistical analysis was performed using GraphPad Prism.

For PK/PD studies, animals were randomized into treatment groups of $n = 3$ per time point for vehicle control and each tested dose with an average tumor size of ~500 mm^3. Animals were treated once (q.d.) and sacrificed at the respective time point. Blood samples and tumor samples for PK and PD analyses were collected, snap-frozen in liquid nitrogen, and stored frozen at –80°C until further processing.

For oral dosing, JDQ443, sotorasib, and adagrasib were formulated in 0.5% methylcellulose/0.1% Tween 80 in water. To assess the effect of continuous dosing on tumor growth, LU99 tumor–bearing nude mice were implanted subcutaneously with a programmable microinfusion pump (iPRECIO, SMP310R, Primetech Corporation) as previously described (56). For this purpose, the catheter connected to the microinfusion pump was inserted into the left external jugular vein via midcervical incision, and the body of the microinfusion pump was implanted subcutaneously on the flank of the mice opposite to the xenograft tumor. For infusion, JDQ443 was dissolved in 30% PEG and 10% Kolliphor at a concentration of 3 and 10 mg/mL. The infusion rate of 4 μL/h was programmed with iPRECIO Management Software v1.0.4.0. Pumps were refilled with vehicle or JDQ443 daily. At days 2 to 3, 9 to 10, and 12 to 13, the drug released was quantified in blood samples collected at the tail vein by LC-MS/MS.

In Vivo *PDX Studies*

Studies were conducted at Southern Texas Accelerated Research Therapeutics (XenoSTART). PDX models were established by direct implantation of patient NSCLC or colorectal cancer tumor tissue subcutaneously into nude mice and were maintained through *in vivo* serial passaging. A cohort of female athymic Crl:NU(NCr)-*Foxn1*^{nu}-homozygous nude mice was implanted subcutaneously with tumor fragments from each PDX model (typically p4–p9). Each individual mouse was assigned to a treatment group for dosing, or to the untreated control group, once its tumor volume reached 200 to 250 mm^3. One animal per PDX model was assigned to each treatment arm according to the 1 × 1 × 1 MCT paradigm (32). Tumor volumes were measured twice weekly by caliper, and body weights were recorded twice weekly. The end of study per model was defined as a minimum 28 days of treatment, or duration for untreated tumor to reach 1,500 mm^3, or duration for two doublings of untreated tumor, whichever was slower. Tumor volume (TV) was calculated as length × width^2/2. The response was determined by comparing tumor volume change at time t with its baseline: ΔTVt = (TVt – TVinitial)/TVinitial × 100%. Tumor growth kinetics in response to treatment is represented by best minimum response (BestMinResponse) and best average response (BestAvgResponse), used to determine the response category for each model. BestMinResponse was defined as the minimum value of ΔTVt for $t \geq 10$ days. For each time t, the average of ΔTVt from $t = 0$ to t was also calculated. BestAvgResponse was the minimum value of this average for $t \geq 10$ days. This metric captures a combination of speed, strength, and durability of response into a single value. The response categories were adapted from RECIST criteria (57) and defined as (in order): complete response = BestAvgResponse <–40% and BestMinResponse <–95%; partial response = BestAvgResponse <–20% and BestMinResponse <–50%; stable disease = BestAvgResponse <30% and BestMinResponse <35%; progressive disease = did not meet any of the criteria above; complete response→progressive disease, partial response→progressive disease,

stable disease→progressive disease were applied if a response was observed but resistance emerged. Mice that were sacrificed because of an adverse event were labeled as "toxic." All data were compiled into a single Spotfire (TIBCO Software Inc.) library. Correlation analyses between data sets were performed within Spotfire. JDQ443 and TNO155 were formulated in 0.5% methylcellulose/0.1% Tween 80 in water. Trametinib was formulated in 0.5% HPMC/0.1% Tween 80 in water. Ribociclib was formulated in 0.5% methylcellulose in water.

Clinical Trial

CJDQ443A12101 (NCT04699188; KontRASt-01) is a phase Ib/II open-label, multicenter dose-escalation and -expansion trial of JDQ443 as a single agent or in combination with TNO155 and/or tislelizumab in adults with *KRAS*^{G12C}-mutated solid tumors previously treated with standard-of-care therapy. The primary objectives of the dose-escalation part were to assess safety and tolerability and to identify the maximum tolerated dose and/or recommended dose and regimen for future studies. JDQ443 monotherapy and the combination of JDQ443 with TNO155 were administered in 21-day cycles. JDQ443 was administered as 100 mg or 200 mg tablets to be taken with food. The trial was conducted in accordance with written Standard Operating Procedures and applicable global/local Good Clinical Practice regulations and International Council for Harmonisation guidelines.

Data Availability

The data generated in these analyses are available within the article and its supplementary data files. Crystallography coordinates have been deposited with the Protein Data Bank for KRAS^{G12C} bound to structures **[2]** (accession #7R0N), **[3]** (7R0Q), and JDQ443 (7R0M). Novartis will not provide access to patient-level data if there is a reasonable likelihood that individual patients could be reidentified. Phase I studies, by their nature, present a high risk of patient reidentification; therefore, individual patient results for phase I studies cannot be shared. In addition, clinical data, in some cases, have been collected subject to contractual or consent provisions that prohibit transfer to third parties. Such restrictions may preclude granting access under these provisions. Where codevelopment agreements or other legal restrictions prevent companies from sharing particular data, companies will work with qualified requestors to provide summary information where possible.

Authors' Disclosures

A. Weiss reports a patent for PCT/CN2021/139694 pending, and is an employee of and stockholder in Novartis. E. Lorthiois reports a patent for WO/2021/124222 pending and a patent for PCT/CN2021/139694 pending, and is an employee of and a stockholder in Novartis. L. Barys is an employee of and a stockholder in Novartis. K.S. Beyer is an employee of and a stockholder in Novartis. C. Bomio-Confaglia is an employee of and a stockholder in Novartis. H. Burks is an employee of and a stockholder in Novartis. X. Chen reports other support from Novartis Pharmaceuticals during the conduct of the study. X. Cui reports a patent for PCT/CN2021/139694 pending, and is an employee of and a stockholder in Novartis. R. de Kanter is an employee of and a stockholder in Novartis. L. Dharmarajan is an employee of and a stockholder in Novartis. C. Fedele is an employee of Novartis. M. Gerspacher reports a patent for WO/2021/124222 pending and a patent for PCT/CN2021/139694 pending, and is an employee of and a stockholder in Novartis. D.A. Guthy is an employee of and a stockholder in Novartis. V. Head is an employee of and a stockholder in Novartis. A. Jaeger is an employee of and a stockholder in Novartis. E. Jiménez Núñez is an employee of and a stockholder in Novartis. J.D. Kearns is an employee of and a stockholder in Novartis. C. Leblanc reports a patent for WO/2021/124222 pending and a patent for PCT/CN2021/139694 pending, and is an employee of and a stockholder in Novartis. S.-M. Maira is an employee of and a stockholder in Novartis. J. Murphy is an employee of and a stockholder in Novartis. H. Oakman is an employee of and a stockholder in Novartis. N. Ostermann is an employee of and a stockholder in Novartis. J. Ottl is an employee of and a stockholder in Novartis. P. Rigollier reports a patent for WO/2021/124222 pending and a patent for PCT/CN2021/139694 pending, and is an employee of and a stockholder in Novartis. D. Roman is an employee of Novartis. C. Schnell is an employee of and a stockholder in Novartis. R. Sedrani is an employee of and a stockholder in Novartis. T. Shimizu reports grants from Novartis during the conduct of the study, as well as grants from Eli Lilly, Loxo Oncology, Daiichi Sankyo, Takeda Oncology, AbbVie, Pfizer, Bristol Myers Squibb, Eisai, AstraZeneca, Incyte, Symbio Pharmaceuticals, Chordia Therapeutics, 3D-Medicine, Five Prime, PharmaMar, and Astellas and personal fees from Taiho, MSD, Chugai Pharmaceutical, AbbVie, Daiichi Sankyo, and Takeda Oncology outside the submitted work. R. Stringer is an employee of and a stockholder in Novartis. A. Vaupel reports a patent for WO/2021/124222 pending and a patent for PCT/CN2021/139694 pending, and is an employee of and a stockholder in Novartis. H. Voshol is an employee of and a stockholder in Novartis. P. Wessels is an employee of and a stockholder in Novartis. T. Widmer is an employee of and a stockholder in Novartis. R. Wilcken reports a patent for WO/2021/124222 pending and a patent for PCT/CN2021/139694 pending, and is an employee of and a stockholder in Novartis. K. Xu is an employee of and a stockholder in Novartis. F. Zecri is an employee of and a stockholder in Novartis. A.F. Farago reports grants and personal fees from Bayer, AstraZeneca, and Genentech and personal fees from Syros, H3 Biomedicine, Pfizer, Merck, Bristol Myers Squibb, and Roche; a patent for PCT/CN2021/139694 pending; and is an employee of and a stockholder in Novartis. S. Cotesta reports a patent for WO/2021/124222 pending and a patent for PCT/CN2021/139694 pending, and is an employee of and a stockholder in Novartis. S.M. Brachmann reports a patent for PCT/CN2021/139694 pending, and is an employee of and a stockholder in Novartis.

Authors' Contributions

A. Weiss: Conceptualization, formal analysis, supervision, validation, investigation, visualization, methodology, writing–original draft, project administration, writing–review and editing. **E. Lorthiois:** Conceptualization, resources, formal analysis, supervision, validation, investigation, methodology, writing–original draft, project administration, writing–review and editing. **L. Barys:** Formal analysis, validation, visualization, writing–original draft, writing–review and editing. **K.S. Beyer:** Formal analysis, supervision, validation, investigation, visualization, methodology, writing–original draft, writing–review and editing. **C. Bomio-Confaglia:** Formal analysis, supervision, validation, investigation, visualization, methodology, writing–review and editing. **H. Burks:** Conceptualization, supervision, visualization, methodology, writing–original draft, project administration, writing–review and editing. **X. Chen:** Formal analysis, validation, investigation, visualization, methodology, writing–original draft, writing–review and editing. **X. Cui:** Formal analysis, validation, investigation, visualization, methodology, writing–original draft, writing–review and editing. **R. de Kanter:** Formal analysis, supervision, validation, investigation, visualization, methodology, writing–original draft, writing–review and editing. **L. Dharmarajan:** Formal analysis, validation, investigation, visualization, methodology, writing–original draft, writing–review and editing. **C. Fedele:** Formal analysis, supervision, validation, investigation, methodology, writing–original draft, writing–review and editing. **M. Gerspacher:** Formal analysis, supervision, validation, investigation, visualization, methodology, writing–review and editing. **D.A. Guthy:** Formal analysis, supervision, validation, investigation, visualization, methodology, writing–original draft, writing–review and editing. **V. Head:**

Formal analysis, supervision, validation, investigation, visualization, methodology, writing–review and editing. **A. Jaeger:** Investigation, visualization, methodology, writing–original draft, writing–review and editing. **E. Jiménez Núñez:** Conceptualization, visualization, project administration, writing–review and editing. **J.D. Kearns:** Formal analysis, supervision, validation, investigation, visualization, methodology, writing–original draft, writing–review and editing. **C. Leblanc:** Formal analysis, supervision, validation, investigation, visualization, methodology, writing–review and editing. **S.-M. Maira:** Conceptualization, resources, formal analysis, supervision, validation, investigation, visualization, methodology, writing–review and editing. **J. Murphy:** Formal analysis, validation, investigation, visualization, methodology, writing–original draft, writing–review and editing. **H. Oakman:** Investigation, visualization, methodology, writing–original draft, writing–review and editing. **N. Ostermann:** Conceptualization, formal analysis, supervision, validation, investigation, visualization, methodology, writing–original draft, writing–review and editing. **J. Ottl:** Formal analysis, supervision, validation, investigation, visualization, methodology, writing–original draft, writing–review and editing. **P. Rigollier:** Formal analysis, supervision, validation, investigation, visualization, methodology, writing–review and editing. **D. Roman:** Formal analysis, supervision, validation, investigation, visualization, methodology, writing–review and editing. **C. Schnell:** Formal analysis, validation, investigation, visualization, methodology, writing–original draft, writing–review and editing. **R. Sedrani:** Conceptualization, resources, formal analysis, supervision, validation, investigation, visualization, writing–review and editing. **T. Shimizu:** Resources, investigation, visualization, writing–review and editing. **R. Stringer:** Formal analysis, supervision, validation, investigation, visualization, methodology, writing–review and editing. **A. Vaupel:** Formal analysis, supervision, validation, investigation, visualization, methodology, writing–review and editing. **H. Voshol:** Resources, formal analysis, supervision, validation, investigation, methodology, writing–original draft, writing–review and editing. **P. Wessels:** Formal analysis, supervision, validation, investigation, visualization, methodology, writing–review and editing. **T. Widmer:** Formal analysis, supervision, validation, investigation, visualization, methodology, writing–review and editing. **R. Wilcken:** Formal analysis, validation, investigation, visualization, methodology, writing–review and editing. **K. Xu:** Formal analysis, validation, investigation, visualization, methodology, writing–original draft, writing–review and editing. **F. Zecri:** Conceptualization, resources, formal analysis, supervision, validation, visualization, writing–review and editing. **A.F. Farago:** Conceptualization, supervision, visualization, methodology, writing–original draft, project administration, writing–review and editing. **S. Cotesta:** Conceptualization, data curation, formal analysis, supervision, validation, investigation, visualization, methodology, writing–original draft, project administration, writing–review and editing. **S.M. Brachmann:** Conceptualization, data curation, formal analysis, supervision, validation, investigation, visualization, methodology, writing–original draft, project administration, writing–review and editing.

Acknowledgments

The authors acknowledge the coinvestigators on the CJDQ44 3A12101 trial, the patients, and the patients' families. Additionally, the authors acknowledge Flavia Adler, Geneviève Albrecht, Eva Altmann, Jessi Ambrose, Dorothee Arz, Peter Aspesi, Daniel Bauer, Pascal Bernet, Andreas Boos, Alexandra Buhles, Christophe Bury, Deborah Cardoso, Elena Cavicchioli, Dongshu Chen, Gaelle Desjonquères, Ursula Duerler, Berengere Dumotier, Solène Dussauge, Dirk Erdmann, Thomas Ferrat, Patrizia Fontana, Felix Freuler, Ernst Freund, Sara Ganzhorn, Jérome Giovannoni, Aurélie Gluck-Gadé, Samuel Haessig, Constanze Hartwieg, Reto Hurschler, Dan Huynh, Zhao Kang, Malika Kazic-Legueux, Jessica Klein, Julia Klopp, Philipp Koeninger, Julia Köhler, Sebastian Kopec, Tina Kottarathil, Mylene Lanter, Mickael Le Douget, Hansjoerg Lehmann, Andreas Lingel, Alexandra Loeffler, Marie-Anne Lozac'h, Rainer Machauer, Robert Mah, Paul Manley, Felipa Mapa, Laetitia Martinuzzi, Lynn McGregor, Joseph McKenna, Morgane Meistertzheim, Marco Meyerhofer, Sandra Molle, Christophe Mura, Guillaume Ngo, Sandro Nocito, Justin Oborski, Tushar Patel, Kerstin Pollehn, Mitko Ristov, Susan Roest, Wendy Rudge, Laurent Sansregret, Francesca Santacroce, Nadine Schneider, Egge Seeberg, Binesh Shrestha, Mickael Sorge, Christelle Stamm, Dario Sterker, Stephan Stutz, Andreas Theuer, Milen Todorov, Fabien Tritsch, Rainer Tschan, Nicolas Warin, Christine Weber, Kayo Yasoshima, Catherine Zimmermann, Florence Zink, and the Piramal chemistry team.

The authors also thank Karin Briner, Jose Duca, Jeffry Engelman, Diana Graus Porta, Peter Hammerman, Francesco Hofmann, Shefali Kakar, Alice Shaw, and Birgit Schoeberl for strategic and/or scientific discussions.

Editorial assistance with the preparation of this manuscript was provided by Nick Fitch of Articulate Science (London, UK), with funding from Novartis Pharmaceuticals.

The costs of publication of this article were defrayed in part by the payment of page charges. This article must therefore be hereby marked *advertisement* in accordance with 18 U.S.C. Section 1734 solely to indicate this fact.

Received February 7, 2022; revised March 14, 2022; accepted April 1, 2022; published first April 11, 2022.

REFERENCES

1. Karnoub AE, Weinberg RA. Ras oncogenes: split personalities. Nat Rev Mol Cell Biol 2008;9:517–31.
2. Mo SP, Coulson JM, Prior IA. RAS variant signalling. Biochem Soc Trans 2018;46:1325–32.
3. Waters AM, Der CJ. KRAS: the critical driver and therapeutic target for pancreatic cancer. Cold Spring Harb Perspect Med 2018;8:a031435.
4. Simanshu DK, Nissley DV, McCormick F. RAS proteins and their regulators in human disease. Cell 2017;170:17–33.
5. Judd J, Abdel Karim N, Khan H, Naqash AR, Baca Y, Xiu J, et al. Characterization of KRAS mutation subtypes in non-small cell lung cancer. Mol Cancer Ther 2021;20:2577–84.
6. Cox AD, Fesik SW, Kimmelman AC, Luo J, Der CJ. Drugging the undruggable RAS: Mission possible? Nat Rev Drug Discov 2014;13:828–51.
7. Palma G, Khurshid F, Lu K, Woodward B, Husain H. Selective KRAS G12C inhibitors in non-small cell lung cancer: chemistry, concurrent pathway alterations, and clinical outcomes. NPJ Precis Oncol 2021;5:98.
8. Lim SM, Westover KD, Ficarro SB, Harrison RA, Choi HG, Pacold ME, et al. Therapeutic targeting of oncogenic K-Ras by a covalent catalytic site inhibitor. Angew Chem Int Ed Engl 2014;53:199–204.
9. Ostrem JM, Peters U, Sos ML, Wells JA, Shokat KM. K-Ras(G12C) inhibitors allosterically control GTP affinity and effector interactions. Nature 2013;503:548–51.
10. Ganguly AK, Wang YS, Pramanik BN, Doll RJ, Snow ME, Taveras AG, et al. Interaction of a novel GDP exchange inhibitor with the Ras protein. Biochemistry 1998;37:15631–7.
11. Taveras AG, Remiszewski SW, Doll RJ, Cesarz D, Huang EC, Kirschmeier P, et al. Ras oncoprotein inhibitors: the discovery of potent, Ras nucleotide exchange inhibitors and the structural determination of a drug-protein complex. Bioorg Med Chem 1997;5:125–33.
12. Ganguly AK, Pramanik BN, Huang EC, Liberles S, Heimark L, Liu YH, et al. Detection and structural characterization of Ras oncoprotein-inhibitors complexes by electrospray mass spectrometry. Bioorg Med Chem 1997;5:817–20.
13. Pautsch A, Vogelsgesang M, Trankle J, Herrmann C, Aktories K. Crystal structure of the C3bot-RalA complex reveals a novel type of action of a bacterial exoenzyme. EMBO J 2005;24:3670–80.

14. Patricelli MP, Janes MR, Li LS, Hansen R, Peters U, Kessler LV, et al. Selective inhibition of oncogenic KRAS output with small molecules targeting the inactive state. Cancer Discov 2016;6:316–29.
15. Hunter JC, Manandhar A, Carrasco MA, Gurbani D, Gondi S, Westover KD. Biochemical and structural analysis of common cancer-associated KRAS mutations. Mol Cancer Res 2015;13:1325–35.
16. Li C, Vides A, Kim D, Xue JY, Zhao Y, Lito P. The G protein signaling regulator RGS3 enhances the GTPase activity of KRAS. Science 2021;374:197–201.
17. Janes MR, Zhang J, Li LS, Hansen R, Peters U, Guo X, et al. Targeting KRAS mutant cancers with a covalent G12C-specific inhibitor. Cell 2018;172:578–89.
18. Canon J, Rex K, Saiki AY, Mohr C, Cooke K, Bagal D, et al. The clinical KRAS(G12C) inhibitor AMG 510 drives anti-tumour immunity. Nature 2019;575:217–23.
19. Hallin J, Engstrom LD, Hargis L, Calinisan A, Aranda R, Briere DM, et al. The KRAS(G12C) inhibitor MRTX849 provides insight toward therapeutic susceptibility of KRAS-mutant cancers in mouse models and patients. Cancer Discov 2020;10:54–71.
20. Skoulidis F, Li BT, Dy GK, Price TJ, Falchook GS, Wolf J, et al. Sotorasib for lung cancers with KRAS p.G12C mutation. N Engl J Med 2021;384:2371–81.
21. Fakih MG, Kopetz S, Kuboki Y, Kim TW, Munster PN, Krauss JC, et al. Sotorasib for previously treated colorectal cancers with KRAS(G12C) mutation (CodeBreaK100): a prespecified analysis of a single-arm, phase 2 trial. Lancet Oncol 2022;23:115–24.
22. Awad MM, Liu S, Rybkin II, Arbour KC, Dilly J, Zhu VW, et al. Acquired resistance to KRAS(G12C) inhibition in cancer. N Engl J Med 2021;384:2382–93.
23. Tanaka N, Lin JJ, Li C, Ryan MB, Zhang J, Kiedrowski LA, et al. Clinical acquired resistance to KRAS^{G12C} inhibition through a novel KRAS switch-II pocket mutation and polyclonal alterations converging on RAS–MAPK reactivation. Cancer Discov 2021;11:1913–22.
24. Zhao Y, Murciano-Goroff YR, Xue JY, Ang A, Lucas J, Mai TT, et al. Diverse alterations associated with resistance to KRAS(G12C) inhibition. Nature 2021;599:679–83.
25. Weiss J, Yaeger RD, Johnson ML, Spira A, Klempner SJ, Barve MA, et al. KRYSTAL-1: adagrasib (MRTX849) as monotherapy or combined with cetuximab (Cetux) in patients (Pts) with colorectal cancer (CRC) harboring a KRASG12C mutation. Ann Oncol 2021;32(suppl_5): S1283–S1346. Abstract nr LBA6.
26. Gandara D, Marrone K, Govindan R, Skoulidis F, Durm G, Clarke J, et al. A phase 1b study evaluating the combination of sotorasib, a KRAS^{G12C} inhibitor, and afatinib, a pan-ErbB tyrosine kinase inhibitor, in advanced KRAS p.G12C mutated non-small cell lung cancer (NSCLC) [abstract]. In: Proceedings of the AACR-NCI-EORTC Virtual International Conference on Molecular Targets and Cancer Therapeutics; 2021 Oct 7–10. Philadelphia (PA): AACR; Mol Cancer Ther 2021;20(12 Suppl):Abstract nr P05-02.
27. Ramalingam S, Fakih M, Strickler J, Govindan R, Li BT, Goldberg S, et al. A phase 1b study evaluating the safety and efficacy of sotorasib, a KRAS^{G12C} inhibitor, in combination with trametinib, a MEK inhibitor, in KRAS p.G12C-mutated solid tumors [abstract]. In: Proceedings of the AACR-NCI-EORTC Virtual International Conference on Molecular Targets and Cancer Therapeutics; 2021 Oct 7–10. Philadelphia (PA): AACR; Mol Cancer Ther 2021;20(12 Suppl):Abstract nr P05-01.
28. Cee VJ, Volak LP, Chen Y, Bartberger MD, Tegley C, Arvedson T, et al. Systematic study of the glutathione (GSH) reactivity of N-arylacrylamides: 1. effects of aryl substitution. J Med Chem 2015;58:9171–8.
29. Barretina J, Caponigro G, Stransky N, Venkatesan K, Margolin AA, Kim S, et al. The Cancer Cell Line Encyclopedia enables predictive modelling of anticancer drug sensitivity. Nature 2012;483:603–7.
30. Kuljanin M, Mitchell DC, Schweppe DK, Gikandi AS, Nusinow DP, Bulloch NJ, et al. Reimagining high-throughput profiling of reactive cysteines for cell-based screening of large electrophile libraries. Nat Biotechnol 2021;39:630–41.
31. Wijeratne A, Xiao J, Reutter C, Furness KW, Leon R, Zia-Ebrahimi M, et al. Chemical proteomic characterization of a covalent KRASG12C inhibitor. ACS Med Chem Lett 2018;9:557–62.
32. Gao H, Korn JM, Ferretti S, Monahan JE, Wang Y, Singh M, et al. High-throughput screening using patient-derived tumor xenografts to predict clinical trial drug response. Nat Med 2015;21:1318–25.
33. Hong DS, Fakih MG, Strickler JH, Desai J, Durm GA, Shapiro GI, et al. KRAS(G12C) inhibition with sotorasib in advanced solid tumors. N Engl J Med 2020;383:1207–17.
34. Mainardi S, Mulero-Sanchez A, Prahallad A, Germano G, Bosma A, Krimpenfort P, et al. SHP2 is required for growth of KRAS-mutant non-small-cell lung cancer in vivo. Nat Med 2018;24:961–7.
35. Nichols RJ, Haderk F, Stahlhut C, Schulze CJ, Hemmati G, Wildes D, et al. RAS nucleotide cycling underlies the SHP2 phosphatase dependence of mutant BRAF-, NF1- and RAS-driven cancers. Nat Cell Biol 2018;20:1064–73.
36. Ruess DA, Heynen GJ, Ciecielski KJ, Ai J, Berninger A, Kabacaoglu D, et al. Mutant KRAS-driven cancers depend on PTPN11/SHP2 phosphatase. Nat Med 2018;24:954–60.
37. Brana I, Shapiro G, Johnson ML, Yu HA, Robbrecht D, Tan DS, et al. Initial results from a dose finding study of TNO155, a SHP2 inhibitor, in adults with advanced solid tumors. J Clin Oncol 39, 2021 (suppl 15; abstr 3005).
38. Ryan MB, Fece de la Cruz F, Phat S, Myers DT, Wong E, Shahzade HA, et al. Vertical pathway inhibition overcomes adaptive feedback resistance to KRAS(G12C) inhibition. Clin Cancer Res 2020;26:1633–43.
39. Puyol M, Martin A, Dubus P, Mulero F, Pizcueta P, Khan G, et al. A synthetic lethal interaction between K-Ras oncogenes and Cdk4 unveils a therapeutic strategy for non-small cell lung carcinoma. Cancer Cell 2010;18:63–73.
40. Mao CQ, Xiong MH, Liu Y, Shen S, Du XJ, Yang XZ, et al. Synthetic lethal therapy for KRAS mutant non-small-cell lung carcinoma with nanoparticle-mediated CDK4 siRNA delivery. Mol Ther 2014;22:964–73.
41. Ho CSL, Tüns AI, Schildhaus HU, Wiesweg M, Grüner BM, Hegedus B, et al. HER2 mediates clinical resistance to the KRAS(G12C) inhibitor sotorasib, which is overcome by co-targeting SHP2. Eur J Cancer 2021;159:16–23.
42. Koga T, Suda K, Fujino T, Ohara S, Hamada A, Nishino M, et al. KRAS secondary mutations that confer acquired resistance to KRAS G12C inhibitors, sotorasib and adagrasib, and overcoming strategies: insights from in vitro experiments. J Thorac Oncol 2021;16:1321–32.
43. Suzuki S, Yonesaka K, Teramura T, Takehara T, Kato R, Sakai H, et al. KRAS inhibitor resistance in MET-amplified KRAS (G12C) non-small cell lung cancer induced By RAS- and non-RAS-mediated cell signaling mechanisms. Clin Cancer Res 2021;27:5697–707.
44. Xue JY, Zhao Y, Aronowitz J, Mai TT, Vides A, Qeriqi B, et al. Rapid non-uniform adaptation to conformation-specific KRAS(G12C) inhibition. Nature 2020;577:421–5.
45. Hata AN, Niederst MJ, Archibald HL, Gomez-Caraballo M, Siddiqui FM, Mulvey HE, et al. Tumor cells can follow distinct evolutionary paths to become resistant to epidermal growth factor receptor inhibition. Nat Med 2016;22:262–9.
46. Sharma SV, Lee DY, Li B, Quinlan MP, Takahashi F, Maheswaran S, et al. A chromatin-mediated reversible drug-tolerant state in cancer cell subpopulations. Cell 2010;141:69–80.
47. Yen I, Shanahan F, Lee J, Hong YS, Shin SJ, Moore AR, et al. ARAF mutations confer resistance to the RAF inhibitor belvarafenib in melanoma. Nature 2021;594:418–23.
48. Fedele C, Li S, Teng KW, Foster CJR, Peng D, Ran H, et al. SHP2 inhibition diminishes KRASG12C cycling and promotes tumor microenvironment remodeling. J Exp Med 2021;218:e20201414.
49. Lou K, Steri V, Ge AY, Hwang YC, Yogodzinski CH, Shkedi AR, et al. KRAS(G12C) inhibition produces a driver-limited state revealing collateral dependencies. Sci Signal 2019;12:eaaw9450.
50. Amodio V, Yaeger R, Arcella P, Cancelliere C, Lamba S, Lorenzato A, et al. EGFR blockade reverts resistance to KRAS(G12C) inhibition in colorectal cancer. Cancer Discov 2020;10:1129–39.
51. Solomon B, Heist RS, Tan DS, Cassier PA, Dooms C, Van Cutsem E, et al. KontRASt: A phase Ib/II, open-label, multi-center, dose-escalation study of JDQ443 in patients with advanced solid tumors harboring the KRAS G12C mutation [abstract]. In: Proceedings of the AACR-NCI-EORTC Virtual International Conference on Molecular

Targets and Cancer Therapeutics; 2021 Oct 7–10. Philadelphia (PA): AACR; Mol Cancer Ther 2021;20(12 Suppl):Abstract nr LBA038.
52. Fishman PN, Pond GR, Moore MJ, Oza A, Burkes RL, Siu LL, et al. Natural history and chemotherapy effectiveness for advanced adenocarcinoma of the small bowel: a retrospective review of 113 cases. Am J Clin Oncol 2006;29:225–31.
53. Ghandi M, Huang FW, Jane-Valbuena J, Kryukov GV, Lo CC, McDonald ER 3rd, et al. Next-generation characterization of the Cancer Cell Line Encyclopedia. Nature 2019;569:503–8.
54. Cerami E, Gao J, Dogrusoz U, Gross BE, Sumer SO, Aksoy BA, et al. The cBio cancer genomics portal: an open platform for exploring multidimensional cancer genomics data. Cancer Discov 2012;2:401–4.
55. Gao J, Aksoy BA, Dogrusoz U, Dresdner G, Gross B, Sumer SO, et al. Integrative analysis of complex cancer genomics and clinical profiles using the cBioPortal. Sci Signal 2013;6:pl1.
56. Tajiri H, Uruno T, Shirai T, Takaya D, Matsunaga S, Setoyama D, et al. Targeting Ras-driven cancer cell survival and invasion through selective inhibition of DOCK1. Cell Rep 2017;19:969–80.
57. Therasse P, Arbuck SG, Eisenhauer EA, Wanders J, Kaplan RS, Rubinstein L, et al. New guidelines to evaluate the response to treatment in solid tumors. European Organization for Research and Treatment of Cancer, National Cancer Institute of the United States, National Cancer Institute of Canada. J Natl Cancer Inst 2000;92:205–16.